BASE PROPERTY OF POTASSIUM SUPPORTED ON

SBA-15 LOADED WITH ALUMINIUM OXIDE AND

ALUMINIUM-LANTHANUM OXIDE AND THEIR

CATALYTIC PERFORMANCE IN

TRANSESTERIFICATION

Nopphawan Bunthiam

A Thesis Submitted in Partial Fulfillment of the Requirements for the

Degree of Master of Science in Chemistry

Suranaree University of Technology

Academic Year 2019

สมบัติความเป็นเบสของโพแทสเซียมบน SBA-15 ที่บรรจุด้วยอะลูมิเนียมออกไซด์และอะลูมิเนียม-แลนทานัมออกไซด์ และความสามารถในการเร่งปฏิกิริยาทรานส์เอสเทอริฟิเคชัน

นางสาวนพวรรณ บุญเทียม

วิทยานิพนธ์นี้เป็นส่วนหนึ่งของการศึกษาตามหลักสูตรปริญญาวิทยาศาสตรมหาบัณฑิต
สาขาวิชาเคมี
มหาวิทยาลัยเทคโนโลยีสุรนารี
ปีการศึกษา 2562

BASE PROPERTY OF POTASSIUM SUPPORTED ON SBA-15 LOADED WITH ALUMINIUM OXIDE AND ALUMINIUM-LANTHANUM OXIDE AND THEIR CATALYTIC PERFORMANCE IN TRANSESTERIFICATION

Suranaree University of Technology has approved this thesis submitted in partial fulfillment of the requirements for a Master's Degree.

Thesis Examining Committee

_____

(Prof. Dr. James R. Ketudat-Cairns)

Chairperson

_____

(Prof. Dr. Jatuporn Wittayakun)

Member (Thesis Advisor)

_____

(Assoc. Prof. Dr. Sanchai Prayoonpokarach)

Member

_____
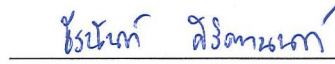
(Asst. Prof. Dr. Threeranun Siritanon)

Member

_____   _____

(Assoc. Prof. Flt. Lt. Dr. Kontorn Chamniprasart)   (Assoc. Prof. Dr. Worawat Meevasana)

Vice Rector for Academic Affairs   Dean of Institute of Science

and Internationalization

นพวรรณ บุญเทียม : สมบัติความเป็นเบสของโพแทสเซียมบน SBA-15 ที่บรรจุด้วย อะลูมิเนียมออกไซด์และอะลูมิเนียม-แลนทานัมออกไซด์ และความสามารถในการเร่ง ปฏิกิริยาทรานส์เอสเทอริฟิเคชัน (BASE PROPERTY OF POTASSIUM SUPPORTED ON SBA-15 LOADED WITH ALUMINIUM OXIDE AND ALUMINIUM-LANTHANUM OXIDE AND THEIR CATALYTIC PERFORMANCE IN TRANSESTERIFICATION) อาจารย์ที่ปรึกษา : ศาสตราจารย์ ดร.จตุพร วิทยาคุณ, 90 หน้า

วิทยานิพนธ์ฉบับนี้ศึกษาความเป็นเบสของโพแทสเซียมฟลูออไรด์ (KF) และโพแทสเซียม ไอโอไดด์ (KI) บนตัวรองรับ 2 ชนิด ได้แก่ SBA-15 บรรจุด้วยอะลูมิเนียมออกไซด์ (Al_2O_3/SBA-15) และอะลูมิเนียมและแลนทานัมออกไซด์ (Al_2O_3-La_2O_3/SBA-15) และใช้ทดสอบความสามารถ ในการเร่งปฏิกิริยาทรานส์เอสเทอริฟิเคชันของกลีเซอริลไตรออกทาโนเอต

การบรรจุโพแทสเซียมลงบน SBA-15 โดยตรงทำให้เกิดการพังของโครงสร้าง SBA-15 ดังนั้นจึงป้องกัน SBA-15 ด้วยการเติม Al_2O_3 ด้วยวิธีเอิบชุ่มเพื่อใช้เป็นตัวรองรับก่อนทำการบรรจุ โพแทสเซียม KF และ KI บน SBA-15 ด้วยวิธีเอิบชุ่มและเผาที่อุณหภูมิ 500 °C เลือกใช้สารตั้งต้น โพแทสเซียมจาก KF และ KI เนื่องจากมีความสามารถในการเร่งปฏิกิริยาทรานส์เอสเทอริฟิเคชัน ได้ดีเมื่ออยู่บน Al_2O_3 จากนั้นศึกษาโครงสร้างของตัวอย่าง KF/Al_2O_3/SBA-15 และ KI/Al_2O_3/SBA-15 ด้วยเทคนิคการเลี้ยวเบนของรังสีเอกซ์ (XRD) การดูดซับและคายซับของแก๊สไนโตรเจน ศึกษา เฟสของโพแทสเซียมบนตัวรองรับด้วยสเปกโทรสโกปีของการดูดกลืนรังสีเอกซ์ที่ใกล้ค่าเอดจ์ (X-ray absorption near edge spectroscopy, XANES) ศึกษาสมบัติความเป็นเบสของวัสดุด้วยการ เปลี่ยนแปลงของเมทิลบิวทานอล (MBOH) ตัวอย่าง KF/Al_2O_3/SBA-15 มีการพังของโครงสร้างและ มีมีโซพอร์ของ SBA-15 ส่วน KI/Al_2O_3/SBA-15 ยังคงมีลักษณะของความเป็นมีโซพอร์เหลืออยู่แม้ว่า จะเกิดการพังของโครงสร้างบางส่วน KI/Al_2O_3/SBA-15 มีความเป็นเบสสูงกว่า KF/Al_2O_3/SBA-15 โดยทำให้ MBOH เกิดการเปลี่ยนแปลง 20%

เพื่อเพิ่มสมบัติความเป็นเบสจึงบรรจุ La_2O_3 บนตัวรองรับ SBA-15 ร่วมกับ Al_2O_3 เนื่องจาก La_2O_3 ทำให้เกิดตำแหน่งซูเปอร์เบสได้ จากนั้นบรรจุ KF และ KI บน Al_2O_3-La_2O_3/SBA-15และเผา ที่อุณหภูมิ 350 และ 500°C สำหรับวัสดุ KF/Al_2O_3-La_2O_3/SBA-15 โครงสร้างและมีโซพอร์ของ SBA-15 ถูกทำลายทั้งหมด สำหรับ KI/Al_2O_3-La_2O_3/SBA-15 มีโซพอร์ยังคงอยู่แม้ว่าจะมีอนุภาค ของ KI เข้าไปอุดตัน KF/Al_2O_3-La_2O_3/SBA-15 เผาที่อุณหภูมิ 350°C ทำให้ MBOH เกิดการ

เปลี่ยนแปลง 50% และความเป็นเบสลดลงเมื่อเผาที่อุณหภูมิ 500°C เนื่องจากการการพังของตัว
รองรับที่มากขึ้น KI/Al$_2$O$_3$-La$_2$O$_3$/SBA-15 15 เผาที่อุณหภูมิ 350°C มีสมบัติความเป็นเบสสูง โดยทำ
ให้ MBOH เกิดการเปลี่ยนแปลง 97-100% อย่างคงที่ตลอดเวลาทดสอบ KI บน Al$_2$O$_3$-La$_2$O$_3$/SBA-
15 เผาที่อุณหภูมิ 500°C เกิดการเสื่อมสภาพตามเวลาทดสอบ เนื่องจากมีเฟสของโพแทสเซียม
ออกไซด์มากขึ้น การบรรจุ La$_2$O$_3$ บนตัวรองรับสามารถปรับปรุงคุณสมบัติความเป็นเบสของวัสดุ
ได้อย่างมีนัยสำคัญ

ส่วนสุดท้ายคือการทดสอบการเร่งปฏิกิริยาทรานส์เอสเทอริฟิเคชัน พบว่าทั้ง
K/Al$_2$O$_3$/SBA-15 และ K/Al$_2$O$_3$-La$_2$O$_3$/SBA-15 ไม่ว่องไวในการเร่งนี้ สำหรับ K/Al$_2$O$_3$/SBA-15 มี
ความสามารถในการเร่งปฏิกิริยาต่ำเพราะมีความเป็นเบสต่ำ K/Al$_2$O$_3$-La$_2$O$_3$/SBA-15 มีความเป็น
เบสสูงแต่เนื่องจาก La$_2$O$_3$ เปลี่ยนเฟสไปเป็น La(CO$_3$)$_3$ ส่งผลให้ความสามารถในการเร่งปฏิกิริยาต่ำ

สาขาวิชาเคมี

ปีการศึกษา 2562

ลายมือชื่อนักศึกษา_____

ลายมือชื่ออาจารย์ที่ปรึกษา_____

NOPPHAWAN BUNTHIAM : BASE PROPERTY OF POTASSIUM SUPPORTED ON SBA-15 LOADED WITH ALUMINIUM OXIDE AND ALUMINIUM-LANTHANUM OXIDE AND THEIR PERFORMANCE IN TRANSESTERIFICATION. THESIS ADVISOR : PROF. JATUPORN WITTAYAKUN, Ph.D. 90 PP.

SBA-15/POTASSIUM/BASE MATERIAL/X-RAY ABSORPTION/ METHYLBUTYNOL CATALYTIC CONVERSION/TRANSESTERIFICATION

This thesis studies the base properties of potassium fluoride (KF) and iodide (KI) on two supports, including SBA-15 loaded with aluminium oxide (Al_2O_3/SBA-15) and aluminium-lanthanum oxide (Al_2O_3-La_2O_3/SBA-15). The prepared materials are tested in transesterification of glyceryl trioctanoate.

A direct loading of potassium on SBA-15 causes a collapse of SBA-15 structure. Thus, SBA-15 is loaded with Al_2O_3 by wetness impregnation and used as a support for potassium. KF and KI are loaded on Al_2O_3/SBA-15 by wetness impregnation and followed by calcination at 500°C. KF and KI are selected as potassium precursors because of their good catalytic activity in transesterification when supporting in Al_2O_3. The structures of materials are analyzed by X-ray diffraction (XRD) and N_2 adsorption-desorption. Phases of potassium on the supports are investigated by X-ray absorption near edge spectroscopy (XANES). The basicity is studied by methylbutynol (MBOH) catalytic conversion. KF/Al_2O_3/SBA-15 results in SBA-15 structure and mesopores collapse. Conversely, KI/Al_2O_3/SBA-15 retains the mesoporous character, although partial destruction occurs. KI/Al_2O_3/SBA-15 has slightly higher basicity than KF/ Al_2O_3/SBA-15 with 20% conversion of MBOH.

To improve the basicity, lanthanum oxide (La_2O_3) is introduced to the support with Al_2O_3, because it could generate superbasic sites. KF and KI are loaded on Al_2O_3-La_2O_3/SBA-15 and calcined at 350 and 500°C. SBA-15 mesostructure is destroyed severely in KF/Al_2O_3-La_2O_3/SBA-15. The mesopores retains in KI/Al_2O_3-La_2O_3/SBA-15, although the loaded KI plugs the pores. KF/Al_2O_3-La_2O_3/SBA-15 calcined at 350°C gives 50% conversion of MBOH and the basicity decreases upon calcination at 500°C, resulting from more collapse of the support. KI/Al_2O_3-La_2O_3/SBA-15 calcined at 350°C has high basicity with MBOH conversion of 97.5% over time on stream. KI/Al_2O_3-La_2O_3/SBA-15 calcined at 500°C deactivates over time on stream as a result of more potassium oxide phase. Loaded La_2O_3 on the support significantly improves the basicity of materials.

All materials are tested in the transesterification reaction. Both K/Al_2O_3/SBA-15 and K/Al_2O_3-La_2O_3/SBA-15 are not active in this reaction. K/Al_2O_3/SBA-15 provides low catalytic performance due to low basicity. For K/Al_2O_3-La_2O_3/SBA-15, it contains high basicity, but La_2O_3 converts to $La_2(CO_3)_3$, resulting in low catalytic performance.

School of Chemistry

Academic Year 2019

Student's Signature _____

Advisor's Signature _____

ACKNOWLEDGEMENTS

I would like to thank these people who participate directly and indirectly in this thesis. I would like to thank Prof. Jatuporn Wittayakun, my advisor, who gave me not only a guidance and support in developing this thesis, but also the instructions to work as a researcher in a future, apart from special appreciation for his kindness, instructions and advice throughout my study in SUT. Prof. Frank Rößner is thanked for his supervision about MBOH reaction testing and supporting reactor and facilities for the experiments at Carl von Ossietzky Universität, Oldenburg, Germany. Besides that, I would like to give him a special thank you for his assistance and advice during stay for my research there. Members in the Catalysis and Chemical Analysis Labs are thanked for their helpful suggestions in the experiments. Members in the Technishe Chemie II are thanked for their help in MBOH reaction testing. Finally, my family and friends are thanked for their care and support during my study.

My study was supported by a Thai scholarship through the Development and Promotion of Science and Technology Talents Project (DPST).

Nopphawan Bunthiam

CONTENTS

CONTENTS (Continued)

CONTENTS (Continued)

LIST OF FIGURES

LIST OF FIGURES (Continued)

LIST OF FIGURES (Continued)

LIST OF FIGURES (Continued)

LIST OF TABLES

CHAPTER I

INTRODUCTION

This research focuses on the preparation and study of the property of base materials, consisting of potassium (K) as an active species supported on mesoporous material, SBA-15. There are several research reports about base catalysts consisting of potassium on microporous materials, including zeolite X (Manadee et al., 2017) and zeolite Y (Supamathanon et al., 2011; 2012; Rakmae et al., 2016). Due to the small pore size of zeolites, the diffusion of bulky molecules of reactants and products may be limited. SBA-15 which has larger pore size than zeolites is selected as a support. To improve the diffusion.

The direct loading of alkali metal salt on SBA-15 causes its structure to collapse. To prevent the collapse, SBA-15 should be loaded with aluminium oxide (Al_2O_3) as an interlayer before the alkali metal precursor (Sun et al., 2010). Accordingly, SBA-15 loaded with Al_2O_3 (Al_2O_3/SBA-15) is applied as support in this work.

The choice of potassium is decided from the information in the literature. KI and KF on Al_2O_3 with calcination at 500°C gave a high catalytic activity in transesterification (Xie and Li, 2006). From the great catalytic performance of KF and KI on Al_2O_3, they are selected as potassium precursors. Al_2O_3/SBA-15 are loaded with 12wt.% K by using KF and KI through wetness impregnation, and calcination at 500°C.

To further improve the basicity, lanthanum oxide (La_2O_3) is added to generate

superbasic sites (Liu et al., 2017b), SBA-15 is loaded with aluminium-lanthanum oxide (Al_2O_3-La_2O_3/SBA-15) before loading with KF and KI, and calcination at 350 and 500°C. The applied calcined temperatures are 350°C according to Liu et al. (2017b) and 500°C to compare the obtained basicity with KI and KF on Al_2O_3/SBA-15.

KF/Al_2O_3/SBA-15, KI/Al_2O_3/SBA-15, KF/Al_2O_3-La_2O_3/SBA-15 and KI/Al_2O_3-La_2O_3/SBA-15 are analyzed by several methods. The phase of potassium on the supports is investigated by X-ray absorption near edge spectroscopy (XANES). The base property of the materials is studied by methylbutynol (MBOH) catalytic conversion. This reaction can distinguish the acid-base property of materials through the catalytic activity on transformation of MBOH (Lauron-Pernot et al., 1991). Moreover, the amount of acid and base sites can be determined through the conversion of MBOH.

Finally, all catalysts, including KF and KI on Al_2O_3/SBA-15 and Al_2O_3-La_2O_3/SBA-15, are tested for transesterification. The reactant of this reaction is triglyceride which is a bulky molecule. SBA-15, which is mesoporous materials, is suitable to apply as support in this reaction. 12wt.% K on zeolite Y prepared from acetate buffer as a potassium precursor with calcination at 500°C gave biodiesel yiled of 72% at 60°C within 2 h from refined palm oil (Rakmae et al., 2016). However, the obtained biodiesel yield is lower than those of 98-99% reported in other literature (Soltani et al., 2017). The low catalytic activity might result from mass transfer limitation. NaY sorption dimensionallity, 0.34 nm (Baerlocher and McCusker, 2007) is smaller than the estimated three-dimension of triglyceride, 2.4 nm (Harrison, 2007). Thus, the diffusion of triglyceride to active sites in the pore of NaY is limited. The prepared base materials with SBA-15, which has larger pore size than triglyceride

molecule, are tested in this transesterification with the condition from Rakmae et al. (2016). However, the applied reactant is changed from refined palm oil to glyceryl trioctanoate to avoid the effects from the other components in oil.
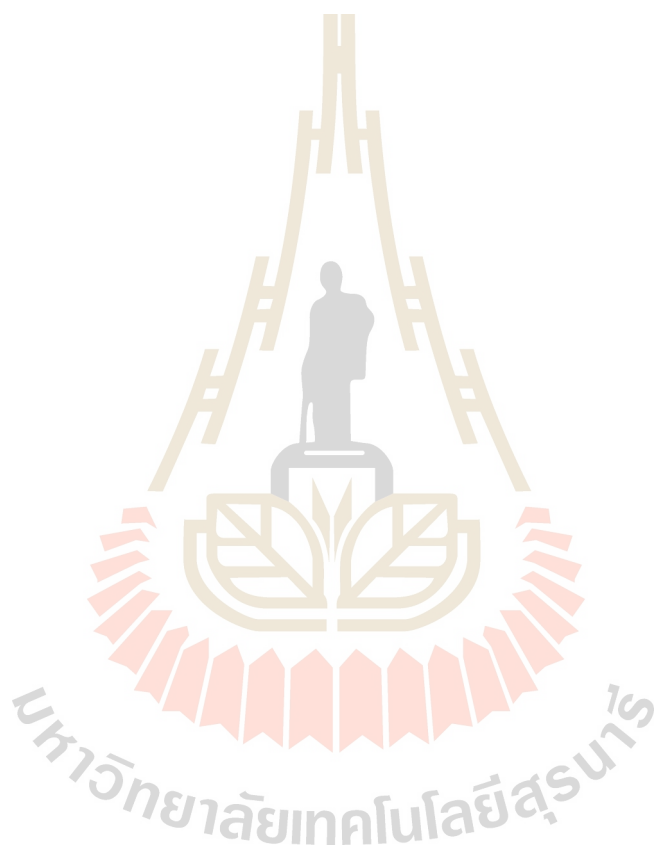
CHAPTER II

LITERATURE REVIEW

2.1 Mesoporous SBA-15

2.1.1 Background

Mesoporous siliceous materials are employed in various fields, including catalysis, separation, adsorption and advanced materials. The wide application is a result from their excellent properties including high surface area (>700 m^2/g), uniform and tunable pore size (2-10 nm), well-defined pore structure and thick pore wall. Santa Barbara Amorphous no. 15, known as SBA-15 has a hexagonal array of pores with a thermal, mechanical and chemical resistance those are appropriate in catalysis (Alothman, 2012). With a large pore size, SBA-15 is selected as a support to reduce mass transfer limitation and improve the catalytic activity of transesterification (Wu et al., 2014; de Lima et al., 2016).

2.1.2 Collapse of SBA-15 by alkali metal

Sun et al. (2008) prepared various catalysts by impregnation of nitrate salts of alkali metal into SBA-15, and then calcination at 550°C to convert the nitrate salt to metal oxide. As a result, the structure of SBA-15 impregnated with alkali precursors collapsed after calcination. They further suggested following reasons for the cause of SBA-15 structure collapse. The first factor is host-guest interaction between oxygen

atoms of SBA-15 (host) and metal atoms of metal oxide (guest). This interaction could well reflect by the electron transfer between oxygen of metal oxides and framework of SBA-15 using the AM1 method in the Gussian 98 program (Sun et al., 2015). If there are strong interaction between guest and host, electron can transfer from alkali metal (guest) to oxygen of SBA-15 (host) easily. Consequently, the collapse of host, SBA-15, was induced. The second reason is mobility in term of diffusion or transfer of formed metal oxide into the pore of silica, which occurs at high temperature. The high mobility leads to the destruction of support. In this case, the mobility of alkali metal oxide is high, thus the structure of SBA-15 was destroyed.

2.1.3 Prevention collapse of SBA-15 from alkali metal by coating metal oxide

Sun et al. (2015) suggested that the collapse of SBA-15 could be prevented by coating with metal oxide interlayer before loading with alkali metal precursor. The metal oxide interlayer can prevent a direct contact between alkali metal and SBA-15. Sun et al. (2010) modified mesoporous silica SBA-15 with Al_2O_3 by 2 methods: direct synthesis (AS(d)) and post synthesis (AS(p)). In the direct synthesis, Al source was added to the template (Pluronic123) together with tetraorthosilicate (TEOS) to form Al-SBA-15. After loading KNO_3, the structure of SBA-15 and Al-SBA-15 collapsed. From this method Al atom located in the framework of SBA-15 and did not prevent a direct contact between K and siliceous framework which is the main reason for the collapse. Figure 2.1 compares structures of SBA-15 and Al-SBA-15 (direct and post synthesis) and changes after the K loading.
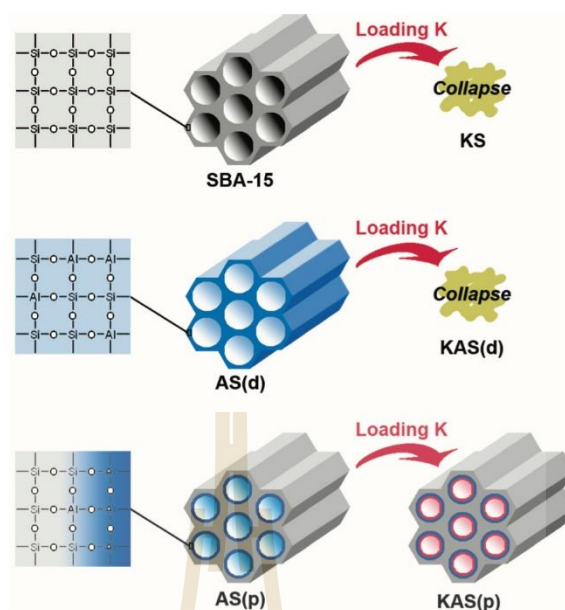
Figure 2.1 Structure of before and after loading K base species into Al_2O_3 modified SBA-15 by direct synthesis AS(d) and post synthesis AS(p) methods (Sun et al., 2010).

In the post synthesis, Al source was introduced to the synthesized SBA-15 to create Al_2O_3 interlayer on SBA-15 which protected a direct contact between K and the siliceous framework. As a result, the structure of SBA-15 was conserved.

Xie and Li (2016) prepared potassium on aluminium oxide by using various potassium precursors. As-synthesized catalysts were calcined at 500°C for 2 h before testing in transesterification. The catalytic activity (conversion) of calcined K/Al_2O_3 ordered by type of potassium precursors is in the order $KI \approx KF > KOH > KNO_3 > K_2CO_3 > KBr$. They also studied the effect of calcination temperature of as-synthesized KI on Al_2O_3 on basicity. The highest basicity was provided at calcined temperature 500°C. At this temperature, KI was partially converted to K_2O after calcination and acted as the active species for transesterification. According to these results, KF and KI

are selected as the potassium precursors due to great catalytic performance on Al_2O_3 and the calcination temperature at 500°C is adopted.

Liu et al. (2017b) designed catalysts with high basicity for ring-opening reaction of propylene oxide with methanol to produce propylene glycol monomethyl ester. The selected support and active species were SBA-15 and KF, respectively. KF was activated by calcination at 350°C before applying in the reaction. Al_2O_3 was coated on SBA-15 before impregnation of KF. They reported that aluminium oxide preserves the framework of SBA-15. However, the obtained material had low basicity with Hammett basic strength 18.4 (see the top route in Figure 2.2). To enhance basicity, La_2O_3 was introduced to SBA-15 to generate solid superbase. After KF was loaded on La_2O_3/SBA-15, the obtained material had high basicity with Hammett basic strength 26.5 (see the middle route in Figure 2.2). However, the structure of SBA-15 collapsed partially. Finally, they found that coating SBA-15 with Al_2O_3 and La_2O_3 before loading with KF can generate superbacity and preserve siliceous framework of SBA-15 (see the bottom route in Figure 2.2). In addition, Al_2O_3 can improve a dispersion of La_2O_3 inside the channels of SBA-15.
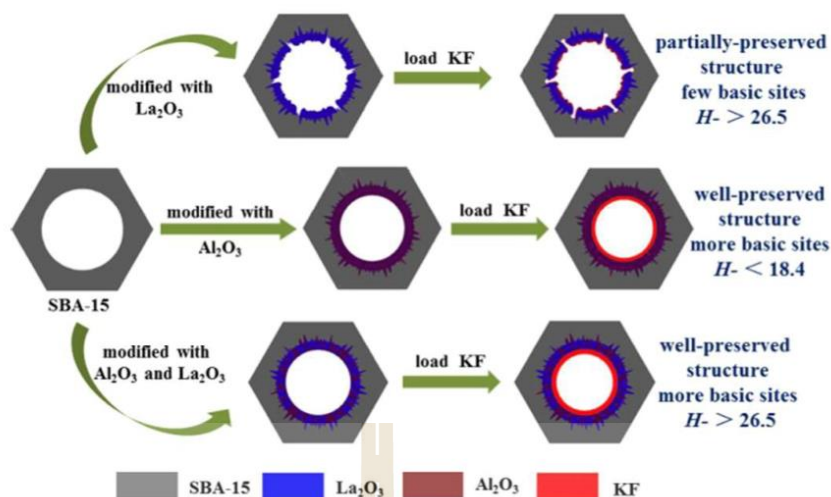
Figure 2.2 The SBA-15 structure before and after modified with Al_2O_3 and La_2O_3 and the structure of modified SBA-15 after loaded with KF (Liu et al., 2017b).

The KF/Al_2O_3-La_2O_3/SBA-15 at Al/La molar ratio was 0.4 had the highest total basicity in amount 0.79 mmol/g and the basic strength H_- 27 identified as superbasic site. The highest catalytic activity was achieved by KF/Al_2O_3-La_2O_3/SBA-15 at this molar ratio. The catalytic activity relates to the increase of basicity of catalyst. Compared with monometallic oxide interlayer catalyst, the KF/Al_2O_3-La_2O_3/SBA-15 catalyst presented significantly higher catalytic activity. It was suggested that the bimetallic oxide of Al and La helps to preserve framework of SBA-15 and improved the catalytic activity.

From excellent properties of KF/Al_2O_3-La_2O_3/SBA-15, it is considered in this work to apply loading the interlayer of Al_2O_3-La_2O_3 enhance the basicity of studied materials before loading with KF and KI. The calcination temperature at 350°C according to Liu et al. (2017) is adopted. Moreover, the calcined temperature at 500°C is performed to compare base property of KF and KI on Al_2O_3-La_2O_3/SBA-15 with those on Al_2O_3/SBA-15.

2.2 Methylbutynol catalytic conversion

An acid and a base property of materials can be studied through the catalytic activity on transformation of methylbutynol (Lauron-Pernot, 1991). 2-methyl-3-butyn-2-ol or methylbutynol (MBOH) can be transformed to the different products, depending on the reaction pathways (Lauron-Pernot, 1991) as shown in Figure 2.3. For the weak acid sites, 3-methyl-3-buten-1-yne (MBYNE) is produced through dehydration of MBOH and for the strong one, 3-methyl-2-buten-1-al (prenal) is generated via isomerization of MBOH. For the coordinatively unsaturated sites or the defect sites, 3-hydroxy-3-methyl-2-butanone (HMB) and 3-methyl-3-buten-2-one (MIPK) are produced. In the base sites, MBOH is decomposed to be acetone and acetylene. From the selectivity of the products from MBOH reaction, it is considered to study the base property of the synthesized materials in this work through the catalytic activity of MBOH transformation.
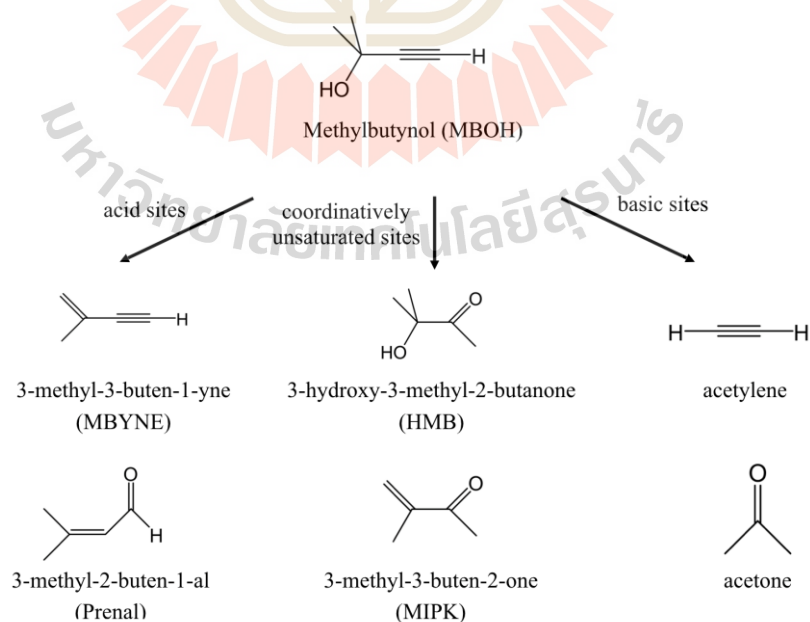
Figure 2.3 Pathways of MBOH reactions.

2.3 Transesterification to produce biodiesel

Biodiesel is produced by transesterification as shown in Equation 2.1. Triglycerides (TG) in oil react with alcohol, generally methanol, by using acid or base catalyst to produce fatty acid methyl esters (FAMES) which is also known as biodiesel (Mansir et al., 2017).

$$
\begin{array}{ccccc}
CH_2\text{-}COOC\text{-}R' & & & R'\text{-}COOCH_3 & CH_2\text{-}OH \\
| & & & & | \\
CH_2\text{-}COOC\text{-}R'' & + 3CH_3OH & \rightleftharpoons & R''\text{-}COOCH_3 & + CH_2\text{-}OH \\
| & & & & | \\
CH_2\text{-}COOC\text{-}R''' & & & R'''\text{-}COOCH_3 & CH_2\text{-}OH
\end{array}
\qquad (2.1)
$$

Triglyceride   **Methanol**   **Methyl ester**   **Glycerol**
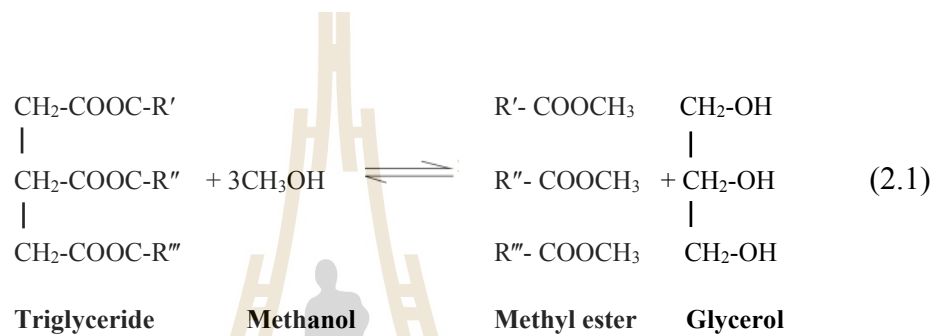
Besides transesterification, oil feedstock with a high amount of free fatty acid (FFA), for example, waste oil and animal fat, can undergo esterification simultaneously by using acid catalyst, Equation 2.2. Other side reactions such as saponification and hydrolysis can also take place to result low biodiesel yield (Soltani et al., 2017).

$$
RCOOH + CH_3OH \rightleftharpoons RCOOCH_3 + H_2O \qquad (2.2)
$$

Fatty acid   **Methanol**   **Methyl ester**   **Water**
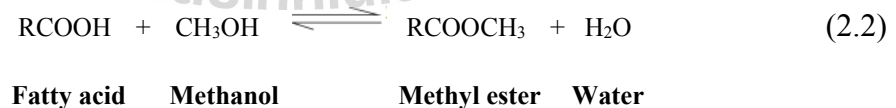
Compared to a conventional diesel, biodiesel has a higher cetane number and lower emission of CO_2, CO, SO_2, particulate matter (PM) and hydrocarbon (HC), less toxicity and better degradability. However, there are some drawbacks of biodiesel, namely lower efficiency on engine speed and power, more deposition of coke on the piston and

head of engine and more degradation and oxidization under long storage time (Ilkılıç et al., 2011; Mahmudul et al., 2017; Roschat et al., 2017). Nevertheless, biodiesel still attracts a lot of attention for research. Catalysts for biodiesel production are widely designed and investigated.

Catalysts in biodiesel production are generally classified to 3 groups: homogeneous, heterogeneous and biocatalyst. The homogeneous and heterogeneous catalysts are categorized into 2 types: acid and base catalyst. The advantages of homogeneous catalyst are high yield and fast rate of reaction. However, they have disadvantages including harsh condition, corrosion of the reactor and a requirement for further purification of products. Heterogeneous catalyst is suitable for industrial application due to its non-corrosive character, reusability, easy and environmental-friendly operation. Heterogeneous catalyst is more attractive than the homogeneous one due to low corrosion, simpler purification of products, easy separation and reusability (Sharma et al., 2011).

An important characteristic of a catalyst in biodiesel production is acid or base properties. There are many types of solid base catalysts for such as metal oxide, mixed metal oxides, zeolite, hydrocalcite, mesoporous material modified by organic components (Sharma et al., 2011). Oxides of alkali and alkaline earth element such as Na, K, Ca, Mg are widely used as active species for transesterification due to their base properties (Sharma et al., 2011). However, one of the main drawbacks is leaching of those oxides in the form of cation into the liquid mixture (Mansir et al., 2017), especially Na, K, Mg, and Ca, (Knothe and Razon, 2017). Among precursors of those metal oxides, potassium compounds are interesting because they are non-toxic, affordable, and producing catalysts with high activity (Lee et al., 2014).

The prepared materials in this work contain base property with potassium as active species. Moreover, the employed support is SBA-15 which has pore size larger than triglyceride molecule. Therefore, the prepared materials are suitable to apply as catalyst in this reaction. They are tested in transesterification to evaluate their catalytic performances.
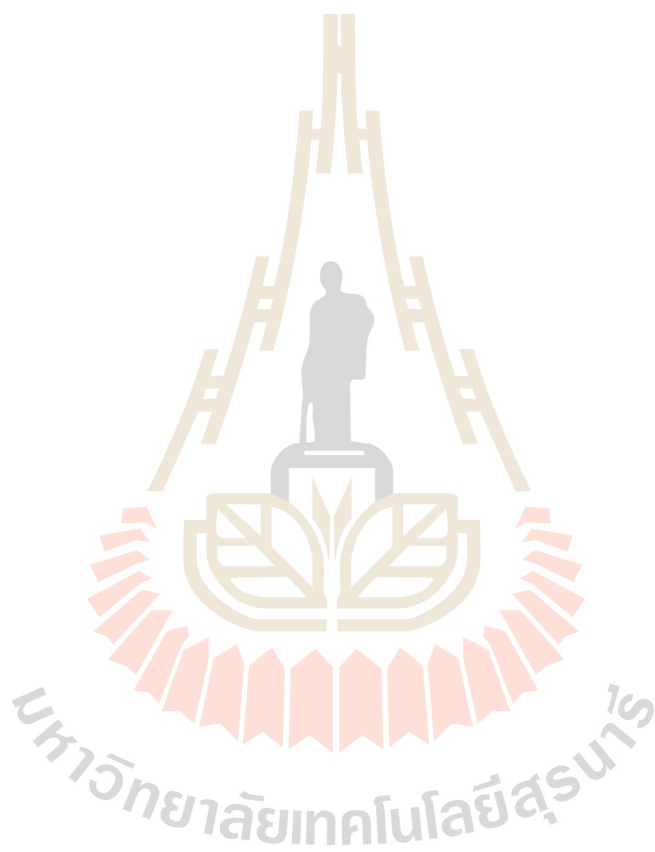
CHAPTER III

MATERIALS AND METHODS

3.1 Chemicals

Chemicals used for SBA-15 synthesis included poly(ethylene glycol)-block-poly(proplylene glycol)-block-poly(ethylene glycol) (P123, $M_n\sim5800$, Sigma-Aldrich), tetraethyl orthosilicate ($Si(OC_2H_5)_4$, TEOS, 98%, Sigma-Aldrich) and hydrochloric acid (HCl, analysis grade, Sigma-Aldrich). Chemicals for preparation of SBA-15 loaded with Al_2O_3 and Al_2O_3-La_2O_3 were aluminium nitrate nonahydrate ($Al(NO_3)_3\cdot9H_2O$, reagent grade, PanReac AppliChem) and lanthanum nitrate hexahydrate ($La(NO_3)_3\cdot6H_2O$, 99.995%, Acros Organics). Chemicals used as potassium precursor were potassium fluoride (KF, analysis grade, Carlo Erba) and potassium iodide (KI, ACS analysis grade, Carlo Erba). Chemicals for transesterification were glyceryl trioctanoate (($CH_3(CH_2)_6COOCH_2)_2CHOCO(CH_2)_6CH_3$), $\geq$99%, Sigma-Aldrich) and methanol (CH_3OH, HPLC grade, Honeywell Riedel-de Haën). The chemicals for analyzing fatty acid methyl ester were methyl octanoate ($CH_3(CH_2)_6COOCH_3$), 99%, Sigma-Aldrich) and methyl nonadecanoate ($CH_3(CH_2)_{17}COOCH_3$, $\geq$98%, Sigma-Aldrich).

3.2 Experimental

3.2.1 Preparation of KF/Al$_2$O$_3$/SBA-15 and KI/Al$_2$O$_3$/SBA-15

SBA-15 was synthesized with the procedure according to Liu et al. (2017b) with slightly adaptation. The synthesis volume was doubled from the original of 75 cm^3 with 2 g of P123 and 4.55 cm^3 of TEOS. The drying temperature was changed from 60°C to 80°C and the calcination time for a complete template removal was increased from 5 h to 6 h. P123 (4 g), a template, was dissolved in 1.6 M HCl (150 cm^3). The mixture was stirred at 40°C for 24 h for complete dissolution. TEOS (9.1 cm^3) was added dropwise into the P123 solution and stirred continuously at 40°C for 24 h. The obtained solution was transferred to a Teflon-lined stainless steel autoclave and aged at 100°C for 24 h. After cooling down, the solid was washed, dried at 80°C, and then calcined at 550°C for 6 h.

SBA-15 was loaded with Al$_2$O$_3$ and Al$_2$O$_3$-La$_2$O$_3$ by wetness impregnation before loading with potassium precursors with following procedure from Liu et al. (2017b). The optimum Al/La molar ratio of 0.4 was applied in this work. SBA-15 (4.0 g) was added to a solution consisting of 3.0 mmol of Al(NO$_3$)$_3$·6H$_2$O (4.5016 g) in ethanol . The mixture was stirred at 40°C for 24 h and heated at 60°C under stirring to remove ethanol. The resulting solid was dried at 60°C and calcined at 550°C for 4 h to obtain the oxide form of Al. The obtained material was denoted as Al$_2$O$_3$/SBA-15.

KF and KI were introduced to the prepared support by wetness impregnation method with the method according to Liu et al. (2017b). The amount of potassium loading was increased from 7.5wt.% in the reference to KF to 12wt.% K in this work. Moreover, the study about potassium iodide as potassium precursor was compared with

potassium fluoride. The calcination temperature at 500°C was further studied in this work besides that at 350°C according to Liu et al. (2017b). The calculated amount of 12wt.% K from KF (0.4054 g) in support was dissolve in methanol. Al_2O_3/SBA-15 (2.0 g) was added into the KF methanol solution and stirred at room temperature for 4 h. Then, methanol was evaporated out at 55°C under stirring. The solid was dried at 60°C and calcined at 500°C for 4 h. The obtained solid was denoted as KF/Al_2O_3/SBA-15, KF represents potassium precursor. KI (1.1582 g) was also impregnated on Al_2O_3/SBA-15 (2 g) with the same procedure. The obtained material was denoted as KI/Al_2O_3/SBA-15.

3.2.2 Preparation of KF/Al_2O_3-La_2O_3/SBA-15 and KI/Al_2O_3-La_2O_3/SBA-15

SBA-15 loaded with Al_2O_3-La_2O_3 was prepared by impregnation using 0.86 mmol of $Al(NO_3)_3 \cdot 6H_2O$ (1.2867 g) and 2.14 mmol of $La(NO_3)_3 \cdot 6H_2O$ (3.7109 g) with the same method of Al_2O_3/SBA-15 preparation. The obtained material was denoted as Al_2O_3-La_2O_3/SBA-15.

The preparation of KF/Al_2O_3-La_2O_3/SBA-15 and KI/Al_2O_3-La_2O_3/SBA-15 were done with the same to that of KF/Al_2O_3/SBA-15 and KI/Al_2O_3/SBA-15. However, as-synthesized KF and KI on Al_2O_3-La_2O_3/SBA-15 were calcined at 2 temperatures: 350°C and 500°C. The synthesized materials were denoted as KF-x/Al_2O_3-La_2O_3/SBA-15 and KI-x/Al_2O_3-La_2O_3/SBA-15 by x is calcination temperature.

3.2.3 Characterization

The synthesized catalysts were analyzed by X-ray diffraction (XRD) on a PANalytical Empyrean with Cu-K$_{\alpha1/\alpha2}$ radiation to characterize the structure of SBA-15. The samples were analyzed at 2θ = 0.5-10 degree (small-angle X-ray diffraction) by using an increment of 0.01°, with a scan speed of 10 s/step and 2θ =10-70 degree by using an increment of 0.02 s/step, with scan speed of 200 s/step respectively.

Adsorption-desorption isotherms were acquired from N$_2$ adsorption-desorption analysis (Micromeritics ASAP2060). The samples were degassed under low pressure around 20 mbar at 60°C, and then analyzed at liquid nitrogen temperature, 196°C. From N$_2$ adsorption-desorption data, total surface was evaluated by Brunauer-Emmett-Teller (BET) equation and pore volume and pore size distribution were calculated by Barrett-Joyner-Halenda (BJH).

The functional groups of SBA-15 before and after modification by loading with metal oxides and potassium were analyzed by attenuated total reflectance Fourier transform infrared spectrometer (Bruker Tensor 27) with resolution 4 cm^{-1}. The samples were placed in the sample holder and pressed by Attenuated Total Reflection (ATR) probe for the measurement.

The oxidation state and phase of potassium and lanthanum in samples were investigated by X-ray absorption near edge structure (XANES) at the beamline 5.2 of the Synchrotron Light Research Institute, Thailand. The energy calibration was made by using KI as a standard. The XANES spectra were analyzed in an energy range of 3585-3695 eV with an energy step of 0.2 eV/step and an acquired time of 1 s/point. The measurements were done in transmission mode at room temperature. The samples in

powder form were packed on Kapton® tape (extra-thin polyethylene film) with frame as a window and attached on the sample holder for the measurement.

To study the basic properties of the synthesized materials, all samples were tested in the catalytic conversion of MBOH. The conversion of MBOH was tested with the procedure and condition modified from Alsawalha (2004). Each sample was sieved to particle size in range 200-315 μm. The sieved sample (200 mg) was packed to the stainless-steel fixed bed reactor and activated under N_2 atmosphere to remove water and CO_2 adsorbed on the surface. The temperature and time for activation process are shown in Table 3.1.

Table 3.1 Activation process of catalysts before testing in MBOH conversion.

Step	Process	N_2 flow rate (cm³/min)	Start – End temperature (°C)	Duration (h)
1	Heating	10	RT - 350	1.30
2	Inertization	10	350	4
3	Cooling	10	350-150	2.00
4	Holding	10	150	Until start reaction

The scheme of the apparatus for MBOH reaction adapted from Alsawalha (2004) is represented in Figure 3.1. After the activation process, the mixture of 90%v/v MBOH and 10 %v/v toluene (as an internal standard) was fed through evaporator to vaporize the liquid mixture. The vapour passed through the bypass (A to B) which

connected directly to the Gas chromatograph (GC) to confirm the steady stream of the mixture. When the stream was constant, the reaction was started by switching to the reactor. The acquired products and remained MBOH were detected by GC (Agilent HP 5890 Series II) equipped with flame ionization detector with Optima wax (polyethylene glycol) column with stationary phase thickness 0.25 μm, inner diameter 320 μm and length 30 m.
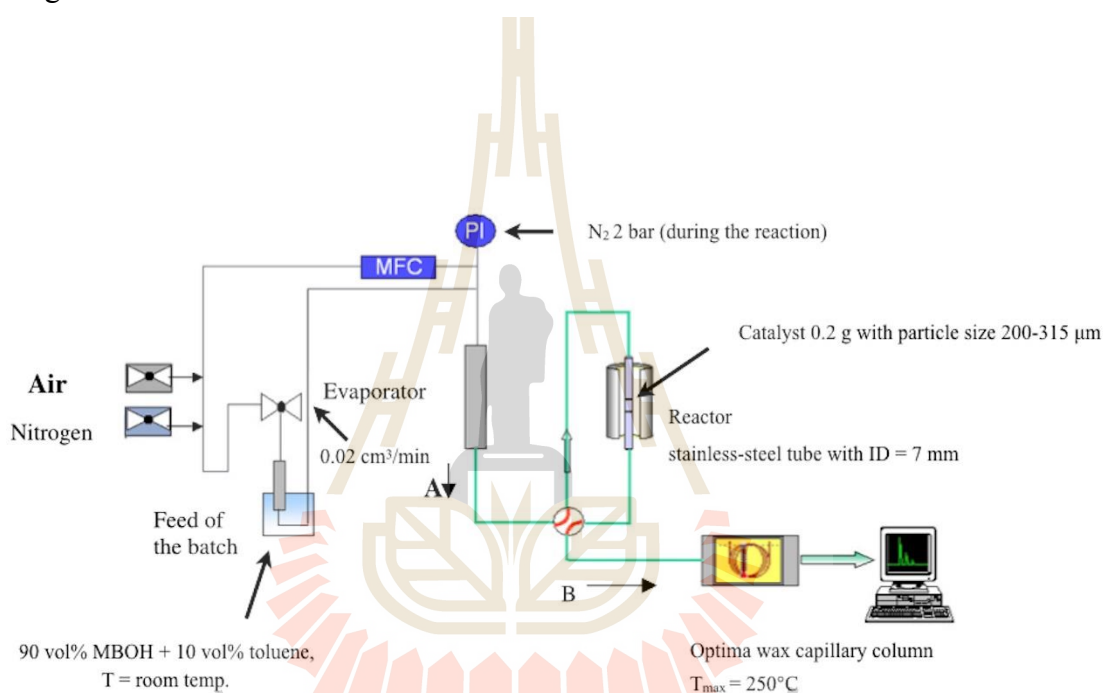
Figure 3.1 The apparatus for the MBOH testing (adapted from Alsawalha, 2004).

Conversion of MBOH, yield and selectivity of each product are calculated from the Equations 3.1, 3.2 and 3.3, respectively (Alsawalha, 2004; Supamathanon et al., 2012).

$$Conversion\ of\ MBOH\ (X_{MBOH})\ = (1 - \frac{A_{MBOH}rRf_{MBOH}/MW_{MBOH}}{\Sigma_{i=1}^{i}A_i rRf_i/MW_i}) \times 100 \quad (3.1)$$

Where A_{MBOH} is the peak area of MBOH

A_i is peak area of each component

rRf_{MBOH} is relative respond factor of MBOH

MW_{MBOH} is molecular weight of MBOH

MW_i is molecular weight of each component

$$Yield\ of\ the\ product\ (Y_p)\ = \frac{A_p rRf_p/MW_p}{\Sigma_{i=1}^{i}A_i rRf_i/MW_i} \times 100 \quad (3.2)$$

Where A_p is the peak area of product

A_i is peak area of each component

rRf_p is relative respond factor of product

MW_p is molecular weight of product

MW_i is molecular weight of each component

$$Selectivity\ of\ the\ product\ (S_p) = \frac{Y_p}{X_{MBOH}} \times 100 \quad (3.3)$$

Where X_{MBOH} is conversion of MBOH

Y_p is yield of product

The relative respond factor is the effect factor in the provided peak area of the chromatogram from the FID detector calculated from Equation 3.4 (de Saint Laumer et al., 2010). The value of effective carbon numbers, molecular weights and calculated relative respond factors are presented in Table 3.2.

$$rRf_i = \frac{ECN_{toluene}/MW_{toluene}}{ECN_i/MW_i}$$ (3.4)

Where $ECN_{toluene}$ is effective carbon of toluene

ECN_i is effective carbon of component i

$MW_{toluene}$ is molecular weight of toluene

MW_i is molecular weight of component i

Table 3.2 The effective carbon numbers (ECN), molecular weights (MW) and relative respond factors (rRf) of all compounds for MBOH reaction testing.

Compound	ECN	rRf	MW (g/mol)
MBOH	5.35	1.19	84.12
Toluene	7.00	1.00	92.14
MBYNE	5.50	0.91	66.10
Prenal	3.90	1.64	84.12
HMB	3.75	2.07	102.13
MIPK	3.90	1.64	86.13
Acetylene	1.95	1.01	26.04
Acetone	2.00	2.21	58.08

3.3 Catalytic activity for transesterification

The synthesized materials were tested for transesterification of glyceryl trioctanoate under the condition from Rakmae et al. (2016). Each catalyst was firstly tested with glyceryl trioctanoate as a model before applying with refined palm oil to avoid the effects from other components in oil. The glyceryl trioctanoate (5 g) was stirred at 250 rpm and heated to 60°C. Then, methanol (2.9 g) and catalyst (0.2 g) was added. The mixture was continuously stirred at 60°C for 2 h. The mixture was hot filtered (Whatman No.5) to separate catalyst from solution. Methanol was removed by a rotary evaporator at 50°C. Then, the solution was transferred into a separatory funnel and left to separate into two layers: remained glyceryl trioctanoate and fatty acid methyl ester (C8) in the upper layer and glycerol in the bottom layer.

The upper layer product was analyzed by GC (Hewlett-Packard 6890) equipped with a flame ionization detector and HP-INNOWax column (crosslinked polyethylene glycol) with stationary phase thickness 0.15 μm, inner diameter 0.32 mm and length 30 m to determine the amount of fatty acid methyl ester (FAME). The amount of FAME in the product was determined by the procedure as described in EN 14103:2011 method with slightly modification. The weight of sample was increased from 100 mg to 150 mg and the amount of solvent was decreased from 10 cm^3 to 1500 μL. Each sample (approximately 150 mg) was dissolved in nonadecanoic acid methyl ester (as an internal standard) in hexane in concentration 10 mg/cm^3 (1500 μL), and then injected to the GC. The initial temperature of the column was 60°C held for 2 minutes, programmed at 10°C/min to 200°C, programmed at of 5°C/min to 240°C held at this temperature for 40 min. The amount of FAME was calculated by using Equation 3.5 according to the EN method and reported in %w/w of FAME in the acquired products.

$$\%FAME\ (\%w/w)\ =\ \frac{A_{C8}}{A_{C19}}\ \times\ \frac{W_{C19}}{W}\ \times\ 100 \tag{3.5}$$

Where A_{C8} is the peak area of octanoic methyl ester

A_{C19} is the peak area of nonadecanoic acid methyl ester

W is the weight of sample in mg

W_{C19} is the weight of nonadecanoic acid methyl ester in mg

The octanoic methyl ester yield was calculated from Equation 3.6 (Rakmae et al., 2016).

$$\%Yield\ =\ \frac{C_{ester}\times n}{\rho_{oil}}\ \times\ 100 \tag{3.6}$$

Where C_{ester} is the concentration of fatty acid methyl ester (C8) in g/cm^3

n is the diluted multiple of octanoic methyl ester (the total volume of n-hexane

divided by the volume of sample)

ρ_{oil} is the density of methyl octanoate in g/cm^3

CHAPTER IV

RESULTS AND DISCUSSION

This chapter is divided to three parts. The first part is the study of structure and basicity of $KF/Al_2O_3/SBA-15$ and $KI/Al_2O_3/SBA-15$ which were calcined at 500°C. The second part is about improving basicity by adding La_2O_3 to produce KF/Al_2O_3-$La_2O_3/SBA-15$ and KI/Al_2O_3-La_2O_3 calcined temperature at 350 and 500°C. The properties of the materials in both parts are analyzed by XRD, N_2 adsorption-desorption and FTIR spectroscopy. Phase of potassium on the support is determined by XAS technique. The base property of materials is studied by MBOH catalytic conversion. The last part is the study of their catalytic performance on transesterification.

4.1 The structure and base property of $KF/Al_2O_3/SBA-15$ and $KI/Al_2O_3/SBA-15$

4.1.1 Results from XRD characterization

Figure 4.1 shows the XRD patterns of SBA-15, $Al_2O_3/SBA-15$, $KF/Al_2O_3/$ SBA-15 and $KI/Al_2O_3/SBA-15$ at low angle. The pattern of SBA-15 shows three peaks corresponding to (100), (110) and (200) planes, characteristic peaks of SBA-15 (Zhao et al., 1998). These planes associate with P6mm hexagonal symmetry (Zhao et al., 1998). The result confirms that SBA-15 was successfully synthesized. The baseline

intensity of samples depends on a width of the light cutdown slit for a low-angle measurement. The characteristic peaks are still observed from Al_2O_3/SBA-15 indicating that the structure of SBA-15 remains after loading Al_2O_3. The shift of the peaks to higher angles suggests that the SBA-15 framework may shrink after loading with Al_2O_3. The shrinkage of the framework may the result from silicate condensation (Wang et al., 2008). The similar result has been reported when SBA-15 are impregnated with magnesium oxide (Wu et al., 2006) and zinc oxide (Wang et al., 2008).
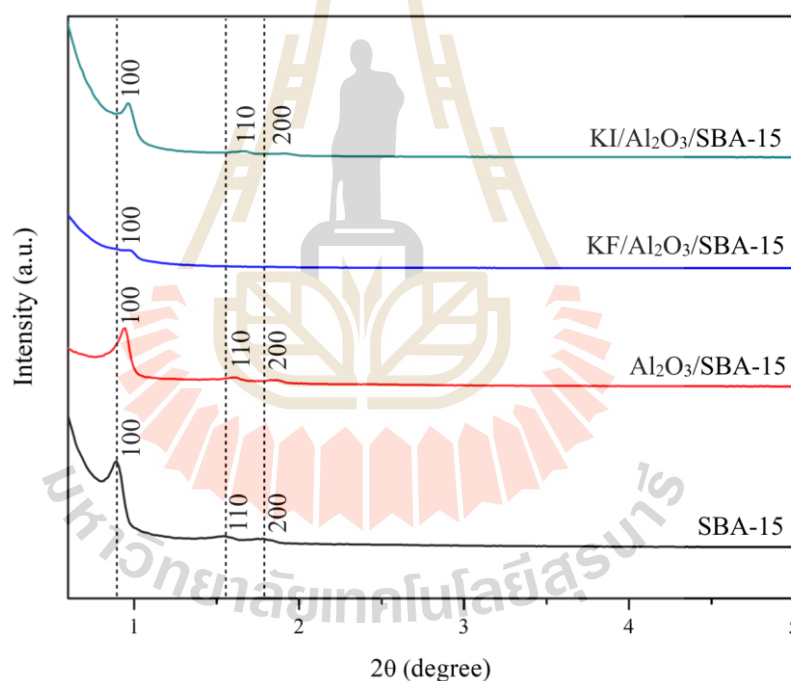
Figure 4.1 XRD patterns at low angle of SBA-15, Al_2O_3/SBA-15, KF/Al_2O_3/SBA-15 and KI/Al_2O_3/SBA-15 calcined at 500°C.

The XRD pattern of KF/Al$_2$O$_3$/SBA-15 shows decrease intensity characteristic peaks suggesting that the structure of Al$_2$O$_3$/SBA-15 may destruct partially after loading with KF. Similar observations have been reported by other researchers (Sun et al., 2010; Liu et al., 2017a). However, the evidence is not clear and, consequently; characterization by other techniques is needed. The pattern of KI/Al$_2$O$_3$/SBA-15 at low angle shows the characteristic peaks of SBA-15 with stronger intensity than that of KF/Al$_2$O$_3$/SBA-15. Therefore, the mesopores structure is better conserved.

The XRD patterns at high angle of SBA-15, Al$_2$O$_3$/SBA-15, KF/Al$_2$O$_3$/SBA-15 and KI/Al$_2$O$_3$/SBA-15 are shown in Figure 4.2. The broad peak around 15°-34° of SBA-15 attributes to amorphous silica phase (Gao et al., 2015). Peaks corresponding to Al$_2$O$_3$ phase are not observed from Al$_2$O$_3$/SBA-15 implying either a good dispersion of Al$_2$O$_3$ or amorphous phase on SBA-15. KF/Al$_2$O$_3$/SBA-15 shows peaks at 29.7°, 36.5° and 42.5° corresponding to K$_3$AlF$_6$ complex (PDF 3-615) from KF and Al of Al$_2$O$_3$ on SBA-15. The result agrees with the work from Handa et al. (1998) and Clacens et al. (2004). When KF was loaded on Al$_2$O$_3$, the phase K$_3$AlF$_6$ was confirmed by XRD and ^{19}F NMR techniques (Clacens et al., 2004). The XRD pattern of KI/Al$_2$O$_3$/SBA-15 shows peaks at 21.7°, 25.1°, 35.9°, 44.3°, 51.8°, 58.3° and 64.6° corresponding to KI phase (PDF 4-471) indicating that KI phase remains after calcination.
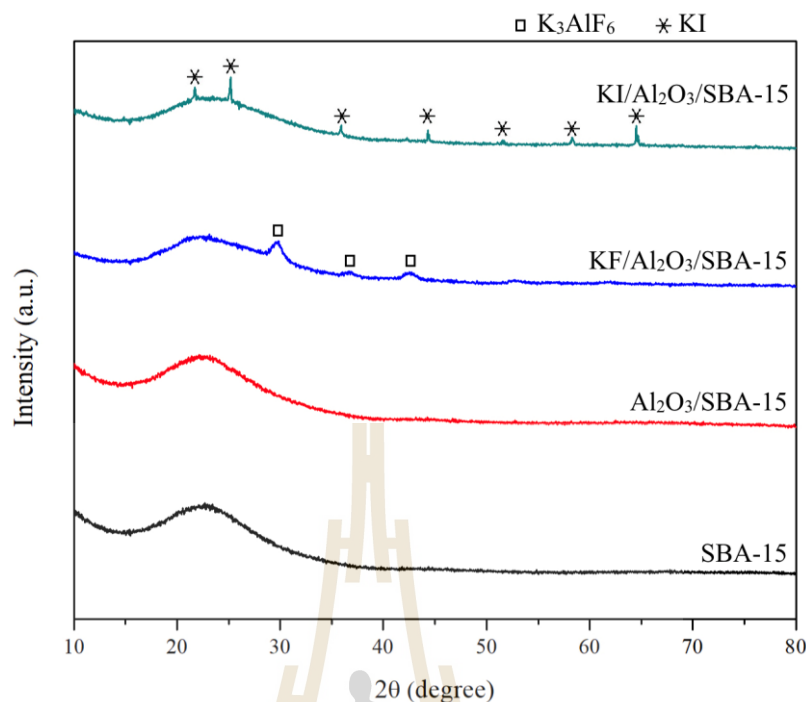
Figure 4.2 XRD patterns at high angle of SBA-15, Al$_2$O$_3$/SBA-15, KF/Al$_2$O$_3$/SBA-15 and KI/Al$_2$O$_3$/SBA-15 calcined at 500°C.

4.1.2 Mesoporous character and surface area

Figure 4.3 shows N$_2$ adsorption-desorption isotherms of all samples. SBA-15 exhibits isotherm type IV which consists of monolayer-multilayer adsorption with hysteresis loop, found in mesoporous materials according to IUPAC technical report (Thommes et al., 2015). The observed hysteresis loop is type H1, found in narrow range of uniform mesopores (Thommes et al., 2015). Compared to SBA-15, Al$_2$O$_3$/SBA-15 has a lower monolayer adsorption and slightly broader hysteresis loop. The observed hysteresis loop confirms that the mesopore character of SBA-15 remains after loading with Al$_2$O$_3$. The broader hysteresis loop implies that Al$_2$O$_3$ disperses in the mesopores of SBA-15. Table 4.1 presents BET surface areas, pore diameters, volumes of mesopore

and micropore and total pore volumes of all samples. The monolayer adsorption, the calculated surface area, the mesopore and micropore volume of Al_2O_3/SBA-15 decrease compared to SBA-15 due to the coverage of SBA-15 surface and mesopores by loaded Al_2O_3.
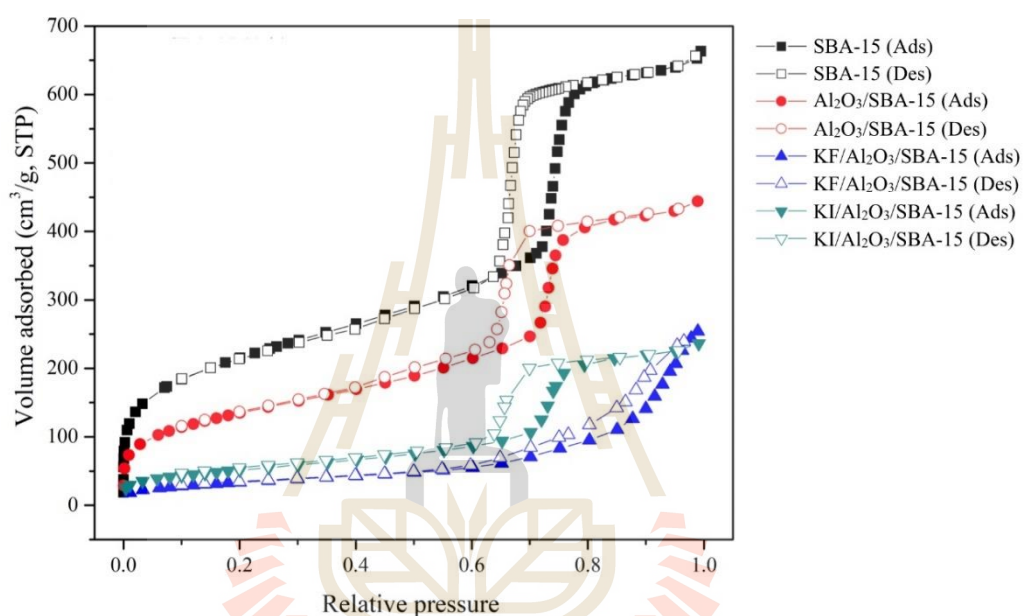
Figure 4.3 N_2 adsorption-desorption isotherms of SBA-15, Al_2O_3/SBA-15, KF/Al_2O_3/ SBA-15 and KI/Al_2O_3/SBA-15 calcined at 500°C.

Table 4.1 BET surface areas (S_{BET}), mesopore volume (V_{meso}), micropore volume (V_{micro}), total pore volume (V_{total}) and pore diameters (D_p) of SBA-15, Al_2O_3/SBA-15, KF/Al_2O_3/SBA-15 and KI/Al_2O_3/SBA-15 calcined at 500°C.

Sample	S_{BET} [a] (m^2/g)	V_{meso} [b] (cm^3/g)	V_{micro} [c] (cm^3/g)	V_{total} (cm^3/g)	D_p [c] (nm)
SBA-15	756	0.94	0.04	0.98	6.2
Al_2O_3/SBA-15	485	0.66	0.01	0.67	5.7
KF/Al_2O_3/SBA-15	122	0.39	-	0.39	12.2
KI/Al_2O_3/SBA-15	186	0.37	-	0.37	6.9

[a]S_{BET} is surface area calculated by BET equation

[b]V_{meso} is mesopore volume calculated by BJH method from the desorption branch

[c]V_{micro} is micropore volume calculated by t-plot method

[c]D_p is average pore diameter calculated by BJH equation from the desorption branch

From KF/Al_2O_3/SBA-15, the adsorbed volume is very low without hysteresis loop (Figure 4.3 and Table 4.1). This observation complements the XRD results confirming the destruction of mesopores of SBA-15. This result agrees well with those reported in the literature (Sun et al., 2010; Liu et al., 2013). The absence of hysteresis loop and a small amount of N_2 adsorption indicate destroyed mesopore structure. Its surface area and pore volume (Table 4.1) are lower than those of SBA-15 resulting from collapse of mesostructure.

KI/Al_2O_3/SBA-15 has low adsorbed volume, but a hysteresis loop is still observed. These indicate that the SBA-15 structure is partially destroyed after loading

KI. A surface area and pore volume of KI/Al$_2$O$_3$/SBA-15 (Table 4.1) also significantly decrease from that of Al$_2$O$_3$/SBA-15. Complement to the XRD results, the structure and mesopores of SBA-15 remains when using KI as potassium precursors although some destruction occurs. In comparison, loading Al$_2$O$_3$/SBA-15 with KF causes more collapse of SBA-15 than with KI.

The pore size distributions of SBA-15, Al$_2$O$_3$/SBA-15, KF/Al$_2$O$_3$/SBA-15 and KI/Al$_2$O$_3$/SBA-15 are shown in Figure 4.4. SBA-15 has a mesopores with narrow distribution agreed with the result from reference synthesis (Liu et al., 2017b). The pore diameter of SBA-15 does not change after loading SBA-15 with Al$_2$O$_3$ and subsequently with KI (Table 4.1), but pore size distribution is broader resulting from dispersion of Al$_2$O$_3$ and KI particles in the pore of SBA-15. Pore distribution is not observed for KF/Al$_2$O$_3$/SBA-15 resulting from the collapse of SBA-15 structure.
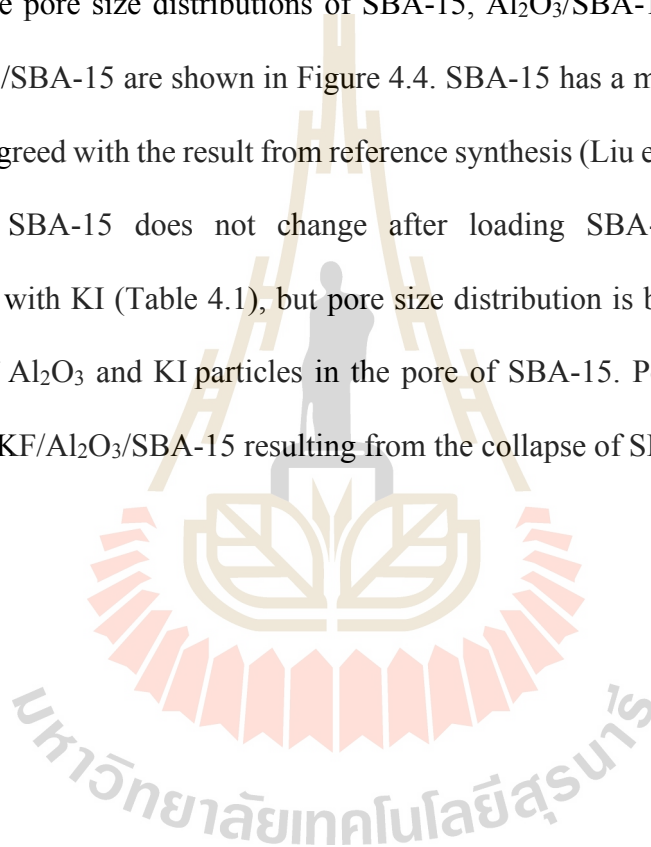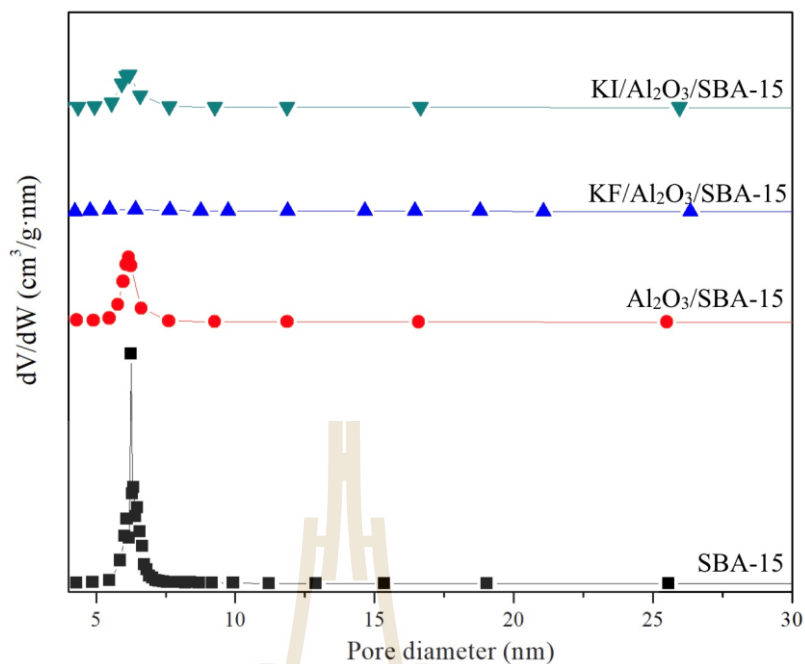
Figure 4.4 Pore size distributions of SBA-15, Al$_2$O$_3$/SBA-15, KF/Al$_2$O$_3$/SBA-15 and KI/Al$_2$O$_3$/SBA-15 calcined at 500°C.

4.1.3 SBA-15 framework and functional groups

Figure 4.5 displays FTIR spectra of SBA-15, Al$_2$O$_3$/SBA-15, KF/Al$_2$O$_3$/ SBA-15 and KI/Al$_2$O$_3$/SBA-15. The spectrum of SBA-15 corresponds to a vibration of SBA-15 framework. A band at 1066 cm^{-1} and peak 795 cm^{-1} attribute to asymmetric and symmetric stretching of Si-O-Si, respectively (Costa et al., 2016). A peak at and 493 cm^{-1} corresponds to Si-O-Si bending (Costa et al., 2016). A peak at 961 cm^{-1} ascribes to bending vibration of silanol groups (Si-OH) (Sun et al., 2010). This peak is not observed from Al$_2$O$_3$/SBA-15 suggesting that almost all silanol groups at surface of SBA-15 reacted with loaded Al$_2$O$_3$. This can confirm a dispersion of Al$_2$O$_3$ in both external and internal surface of SBA-15 (Sun et al., 2010). This assures that almost all surface of SBA-15 was protected by Al$_2$O$_3$ before loading with KF and KI. A direct

contact between potassium and SBA-15 framework must be avoided because potassium causes the complete collapse of SBA-15 structure (see Appendix). Spectra of KF/Al$_2$O$_3$/SBA-15 and KI/Al$_2$O$_3$/SBA-15 are similar to that of Al$_2$O$_3$/SBA-15. KF/Al$_2$O$_3$/SBA-15 spectrum still shows vibration peaks of Si-O-Si and Si-O despite the collapse of SBA-15 structure. However, a peak at 568 cm^{-1} corresponding to O-Si-O bending (Decottignies et al., 1978) is observed from KF/Al$_2$O$_3$/SBA-15. This peak relates to network defects of fused quartz and also found in Raman spectrum of silica gel calcined at 400-800°C (Bertoluzza et al., 1982).

A peak around 1636 cm^{-1} attributing to H$_2$O bending (Costa et al., 2016) is observed from all samples suggesting that the materials could absorb a small amount of water. A peak at 2324 cm^{-1} corresponding to stretching of C-O of CO$_2$ molecule (Costa et al., 2016) is observed form SBA-15 and KF/Al$_2$O$_3$/SBA-15. This is consistent with the literature that a small amount of CO$_2$ could absorb on bare SBA-15 (Saad et al., 2016).
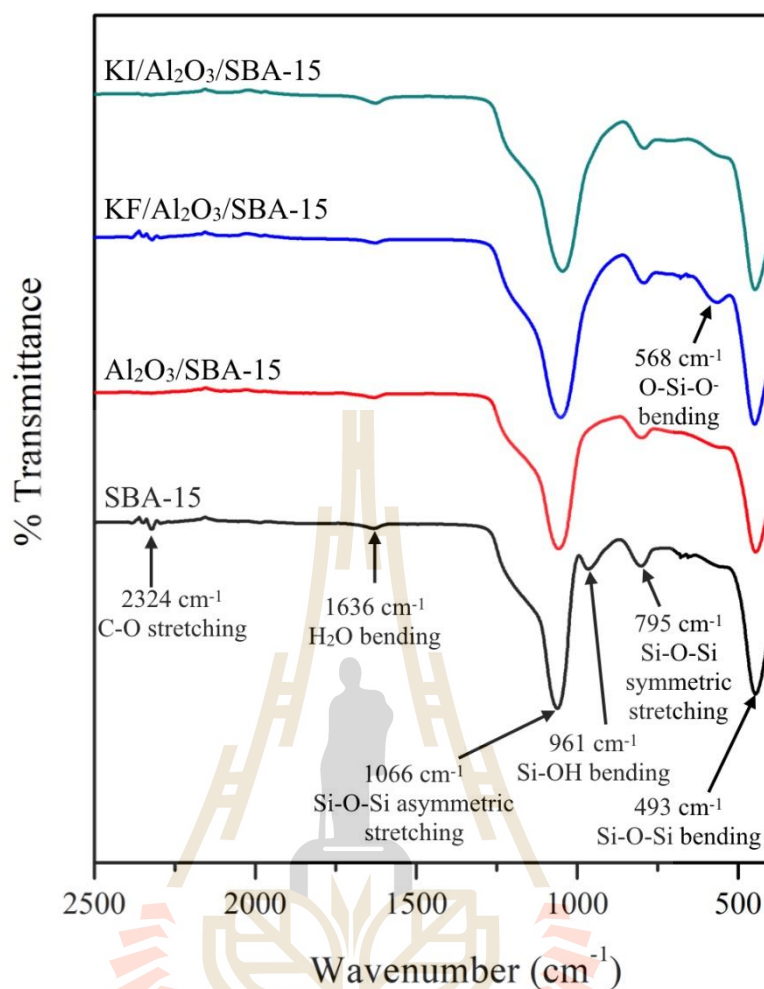
Figure 4.5 FTIR spectra of SBA-15, Al_2O_3/SBA-15, KF/Al_2O_3/SBA-15 and KI/Al_2O_3/SBA-15 calcined at 500°C.

4.1.4 Identification of phase of loaded potassium

Realization of potassium phase on Al_2O_3/SBA-15 is necessary, because it helps to understand their base property. The materials were analyzed by XANES at potassium K-edge to identify potassium phase on support. Figure 4.6 displays XANES spectra of standard KF, standard K_2O and KF/Al_2O_3/SBA-15. Table 4.2 presents their absorption edge energies. Potassium in KF/Al_2O_3/SBA-15 has the same edge energy as

that in standard KF and K_2O indicating that potassium in $KF/Al_2O_3/SBA$-15 has oxidation state +1. The absorption feature of $KF/Al_2O_3/SBA$-15 is compared to standard KF and K_2O to identify the potassium phase. The feature of $KF/Al_2O_3/SBA$-15 spectrum is similar to that of standard KF suggesting that potassium in $KF/Al_2O_3/SBA$-15 is in KF phase.
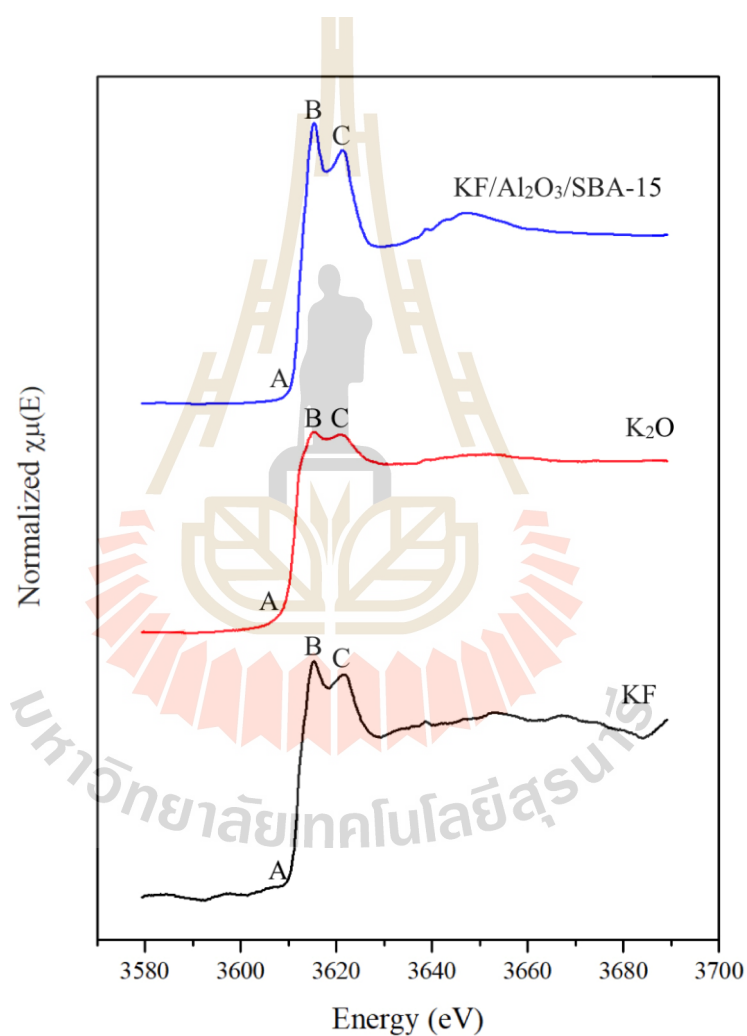
Figure 4.6 XANES spectra of standard KF and K_2O and $KF/Al_2O_3/SBA$-15 calcined at 500°C.

Table 4.2 The absorption edge energies of standard KF, KI and K_2O and KF/Al_2O_3/SBA-15 and KF/Al_2O_3/SBA-15 calcined at 500°C.

Sample	Edge energy (eV)
KF	3612.0
KI	3612.7
K_2O	3611.7
KF/Al_2O_3/SBA-15	3612.2
KI/Al_2O_3/SBA-15	3612.1

Peaks of XANES spectra are assigned in these symbols for discussing about KF particle size on support: edge energy assigned to A, white line assigned to B and the following peak assigned as C. Peak C position shifts from 3621.9 eV for standard KF to 3621.5 eV for KF/Al_2O_3/SBA-15. Jacobs et al. (2017) have reported about relationship between change of peak C position and particle size of potassium. They have compared potassium K-edge XANES spectra of potassium compounds loaded on SiO_2 with the bulk of potassium compounds. The peak C of K/SiO_2 shifted to lower energy and shifts to lower energy of 0.4-0.5 eV when decreasing loading amount of potassium compound from 2.38% to 0.97%. According to this literature, the peak C of KF/Al_2O_3/SBA-15 shifts to lower energy due to a smaller particle size of KF when it was loaded on the support.

Figure 4.7 shows XANES spectra of standard KI and K_2O and KI/Al_2O_3/SBA-15. The edge energy of KI/Al_2O_3/SBA-15 is similar to that of standard KI and K_2O (Table 4.2) indicating that potassium in KI/Al_2O_3/SBA-15 has oxidation

state +1. The spectrum of KI/Al$_2$O$_3$/SBA-15 is similar to that of K$_2$O with slightly feature of KI suggest that potassium in KI/Al$_2$O$_3$/SBA-15 composes of K$_2$O as a major phase and KI as a minor phase. However, the white lines of KI/Al$_2$O$_3$/SBA-15 and K$_2$O are different. The white line of KI/Al$_2$O$_3$/SBA-15 is similar to that of 0.2(Al$_2$O$_3$)·0.8(K$_2$O·3SiO$_2$) glass (Kamijo et al., 1996). Thus, it is possible that K$_2$O on Al$_2$O$_3$/SBA-15 has a strong interaction with Al$_2$O$_3$ and SiO$_2$ which is a composition of SBA-15.
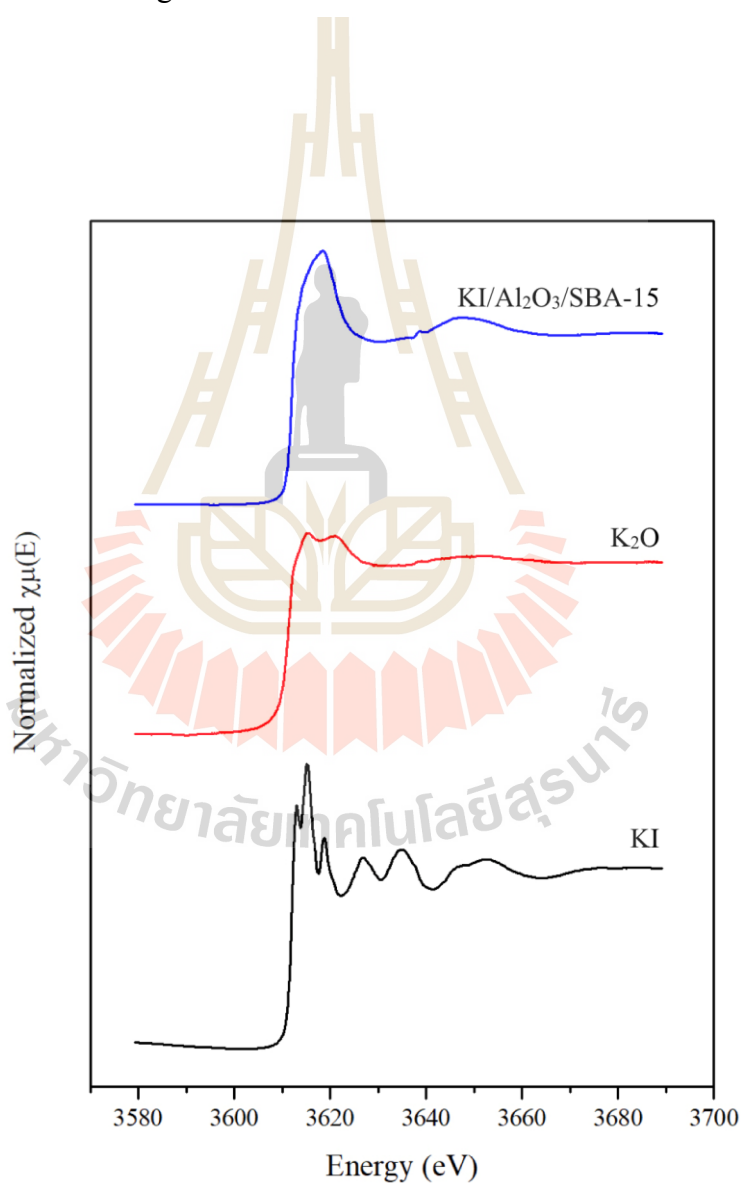
Figure 4.7 XANES spectra of standard KI and K$_2$O and KI/Al$_2$O$_3$/SBA-15 calcined at 500°C.

4.1.5 Study of base property

Figure 4.8 shows conversion of MBOH over SBA-15, Al_2O_3/SBA-15, KF/ Al_2O_3/SBA-15 and KI/Al_2O_3/SBA-15. MBOH hardly converted over SBA-15 indicating that SBA-15 does not contain any acid and base sites. MBOH conversion over Al_2O_3/SBA-15 is 100% at the beginnig and then decreases gradually with the time on stream indicating that the catalyst deactivates during reaction. This results agree well with the literature that acid materials tend to deactivate in MBOH reaction (Kuśtrowski et al., 2004). The MBOH conversion from KI/Al_2O_3/SBA-15 is around 20% and slightly higher than KF/Al_2O_3/SBA-15. Therefore, KI/Al_2O_3/SBA-15 contains slightly higher amount of base sites than that of KF/Al_2O_3/SBA-15.
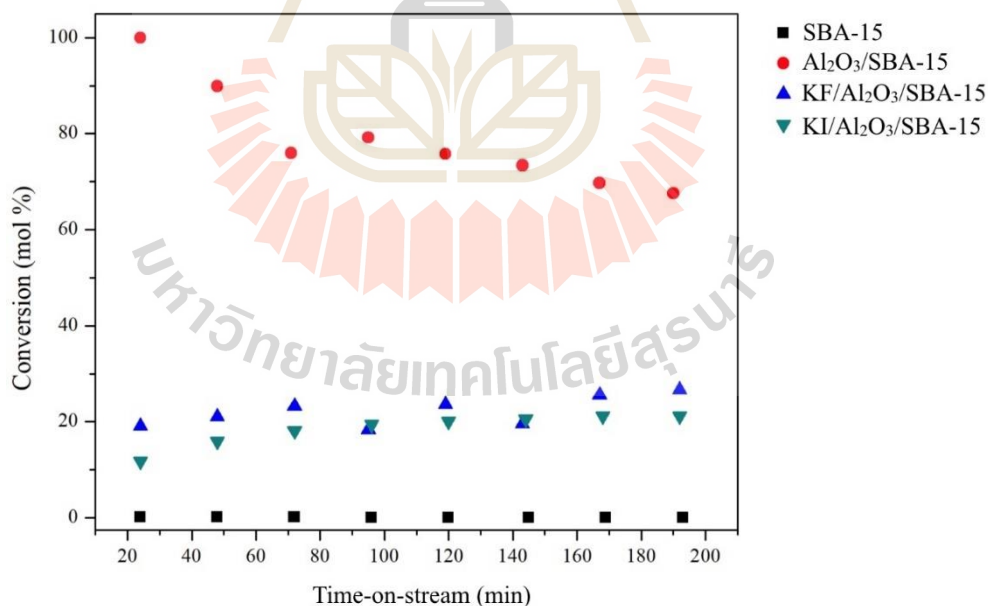
Figure 4.8 Conversion of MBOH over SBA-15, Al_2O_3/SBA-15, KF/Al_2O_3/SBA-15 and KI/Al_2O_3/SBA-15, reaction temperature 150°C.

Figure 4.9 and 4.10 show selectity of acetylene and acetone, respectively. The main product from SBA-15 was MIPK from coordinatively unsaturated or defect sites of the catalyst. The main product from Al_2O_3/SBA-15 was MBYNE produced from the acid pathway with selectivity around 96%. The other products were acetyelene, acetone, and prenal and MIPK in small amouts. Therefore, Al_2O_3/SBA-15 contains mostly acid sites. The obtained products from KF/Al_2O_3/SBA-15 and KI/Al_2O_3/SBA-15 were acetylene and acetone from base pathway confirming that both samples contain base sites. The acid sites of Al_2O_3/SBA-15 is suppressed after loading with potassium. A molar ratio of acetylene and acetone is 0.9 for both materials slightly deviating from one which is the theoritical value. Moreover, selectivity of acetone is significantly lower than acetylene at the beginning of reaction from KF/Al_2O_3/SBA-15. According to Cosimo and Apesteguía (1998) and Aramendia et al. (1999), acetone molecules can undergo condensation and Michael addition reaction. Thus, the amount of acetone decreases.
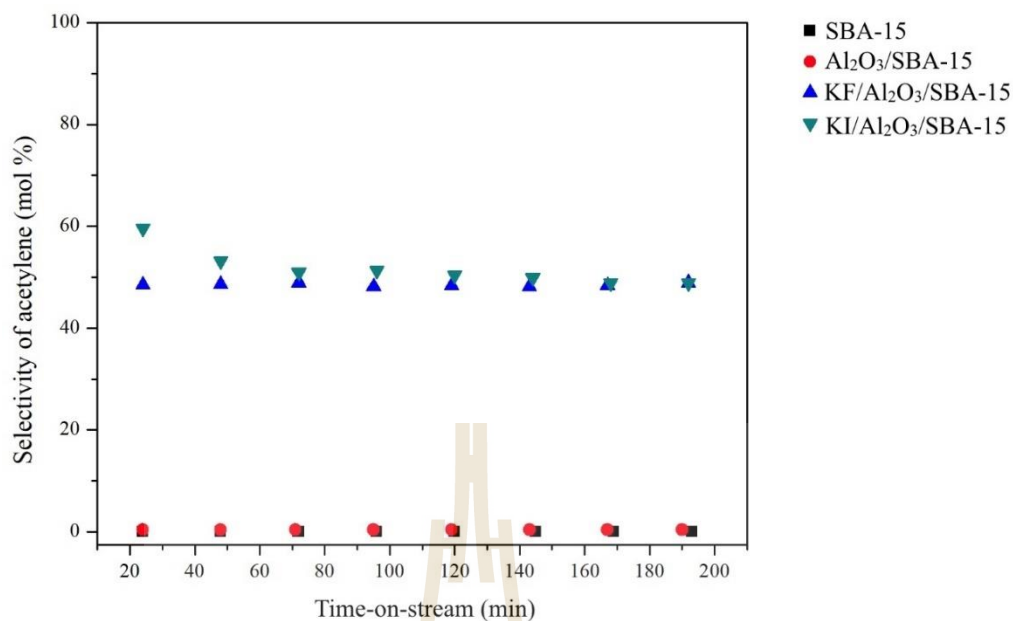
Figure 4.9 Selectivity of acetylene over SBA-15, Al$_2$O$_3$/SBA-15, KF/Al$_2$O$_3$/SBA-15 and KI/Al$_2$O$_3$/SBA-15, reaction temperature 150°C.
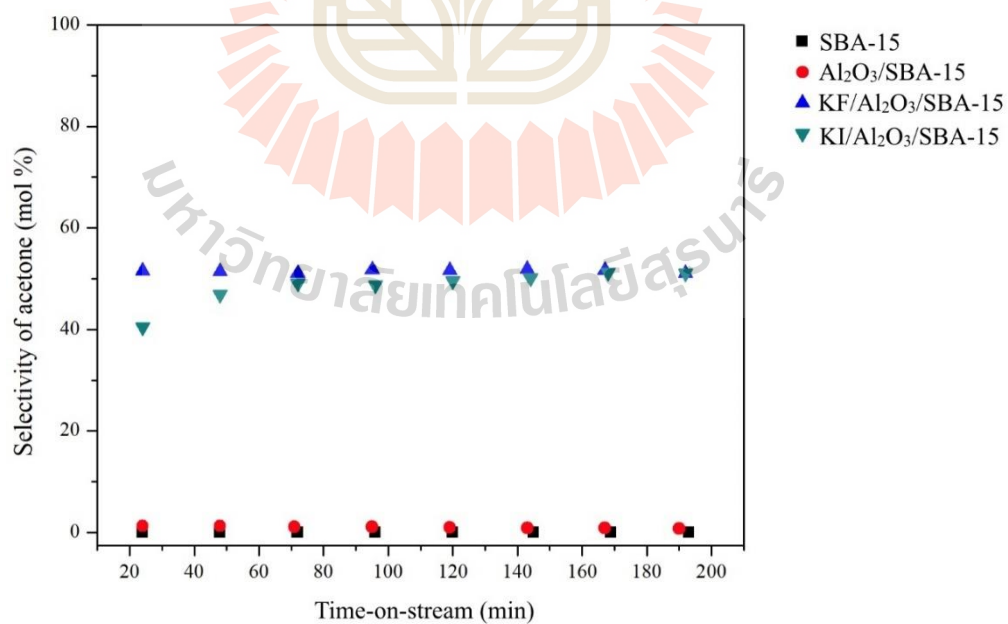
Figure 4.10 Selectivity of acetone over SBA-15, Al$_2$O$_3$/SBA-15, KF/Al$_2$O$_3$/SBA-15 and KI/Al$_2$O$_3$/SBA-15, reaction temperature 150°C.

The results from XRD, N_2 adsorption-desorption and IR techniques indicate that SBA-15 structure collapse for $KF/Al_2O_3/SBA-15$ as the structure partially destructed for $KI/Al_2O_3/SBA-15$. XANES results suggest that potassium in $KF/Al_2O_3/SBA-15$ is KF phase and is in K_2O as major phase and KI as minor phase from $KI/Al_2O_3/SBA-15$. However, the basicity of $KF/Al_2O_3/SBA-15$ and $KI/Al_2O_3/SBA-15$ is slightly different and the amount of base sites is low. Consequently, it is worthwhile to improve the basicity. The next section is about improving base property of materials by introducing La_2O_3 on the support.

4.2 The structure and base property of KF/Al_2O_3-$La_2O_3/SBA-15$ and KI/Al_2O_3-$La_2O_3/SBA-15$

4.2.1 XRD characterization

Figure 4.11 shows XRD patterns of SBA-15, Al_2O_3-$La_2O_3/SBA-15$, KF-350/Al_2O_3-$La_2O_3/SBA-15$ and KF-500/Al_2O_3-$La_2O_3/SBA-15$. At low angle (Figure 4.11(a)), the characteristic peaks of SBA-15 (see detail in section 4.1.1) are observed from Al_2O_3-$La_2O_3/SBA-15$ indicating that the structure of SBA-15 remains after loading with Al_2O_3-La_2O_3. However, the low intensity implies the collapse of SBA-15 structure. Another possibility is that Al_2O_3-La_2O_3 prevents the incident X-ray beam to strike on SBA-15 phase. Moreover, the characteristic peaks shift to higher degree indicating the shrinkage of SBA-15 framework after loading with those metal oxides (see discussion in section 4.1.1). The result agrees well with the reference synthesis (Liu et al., 2017b). At high angle (Figure 4.11(b)), the characteristic peaks of Al_2O_3 and La_2O_3 are not observed implying a good dispersion of those metal oxides in SBA-15.

The characteristic peaks of SBA-15 are not observed from both KF-350/Al_2O_3-La_2O_3/SBA-15 and KF-500/Al_2O_3-La_2O_3/SBA-15. This points out to the collapse of SBA-15 structure after loading KF, similar to the collapse of structure in the literatures (Wu et al., 2006; Sun et al., 2008; Liu et al., 2013). However, more characterization is needed to confirm the structure collapse.

The patterns of KF-350/Al_2O_3-La_2O_3/SBA-15 and KF-500/Al_2O_3-La_2O_3/SBA-15 at high angle show peaks at 27.3, 39.6, 42.9, 48.3 and 56.0° corresponding to La(OH)$_3$ (PDF 6-585). For KF-500/Al_2O_3-La_2O_3/SBA-15, additional peaks at 15.7° and 26.0° are observed corresponding to La(OH)$_3$ (PDF 6-585) and $La_2O_2CO_3$ (PDF 19-650), respectively. Wang et al. (2006) have reported that La_2O_3 could react with H_2O and CO_2 to produce La(OH)$_3$. According to this literature, La_2O_3 in this work could react with moisture and CO_2 in air to produce La(OH)$_3$ in KF-350/Al_2O_3-La_2O_3/SBA-15 and KF-500/Al_2O_3-La_2O_3/SBA-15. La(OH)$_3$ could convert to $La_2O_2CO_3$ by calcination at 500°C (Wang et al., 2014). Therefore, $La_2O_2CO_3$ is observed for KF-500/Al_2O_3-La_2O_3/SBA-15. The peaks corresponding to KF are not observed. Consequently, it is necessary to use other technique to identify the potassium phase.
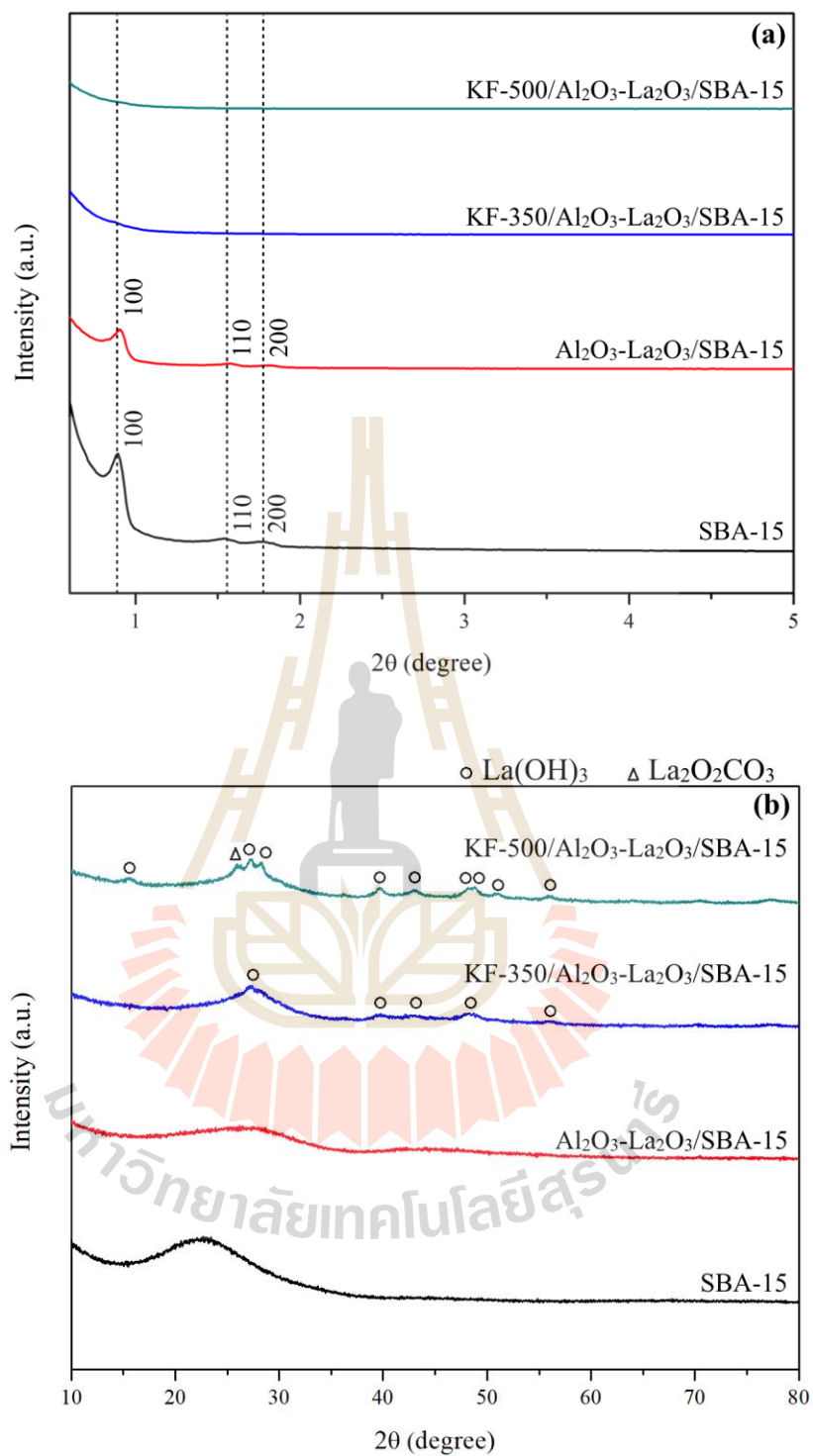
Figure 4.11 XRD patterns at (a) low angle and (b) high angle of SBA-15, Al_2O_3-La_2O_3/ SBA-15, KF-350/Al_2O_3-La_2O_3/SBA-15 and KF-500/Al_2O_3-La_2O_3/SBA-15 (KF supported on Al_2O_3-La_2O_3/SBA-15 calcined at 350 and 500°C).

Figure 4.12 shows XRD patterns of SBA-15, Al_2O_3-La_2O_3/SBA-15, KI-350/Al_2O_3-La_2O_3/SBA-15 and KI-500/Al_2O_3-La_2O_3/SBA-15. The patterns of SBA-15 and Al_2O_3-La_2O_3/SBA-15 are the same as in Figure 4.11. At low angle (Figure 4.12(a)), all characteristic peaks of SBA-15 are observed from KI-350/Al_2O_3-La_2O_3/SBA-15, but only the main peak is observed for KI-500/Al_2O_3-La_2O_3/SBA-15. These results suggest that SBA-15 structure may be partially destroyed after loading with KI. Nevertheless, more characterization is needed. The characteristic peaks shift indicating the shrinkage of SBA-15 framework after loading KI, similar result from SBA-15 loaded with Al_2O_3 and Al_2O_3-La_2O_3. Thus, the calcination can cause the condensation of silicate. The patterns at high angle of both samples (Figure 4.12(b)) show peaks corresponding to KI (PDF 4-471) indicating that KI phase remained in both samples. However, the intensity decreases with the calcination temperature suggesting that KI tends to convert to another phase when it was calcined at 500°C.
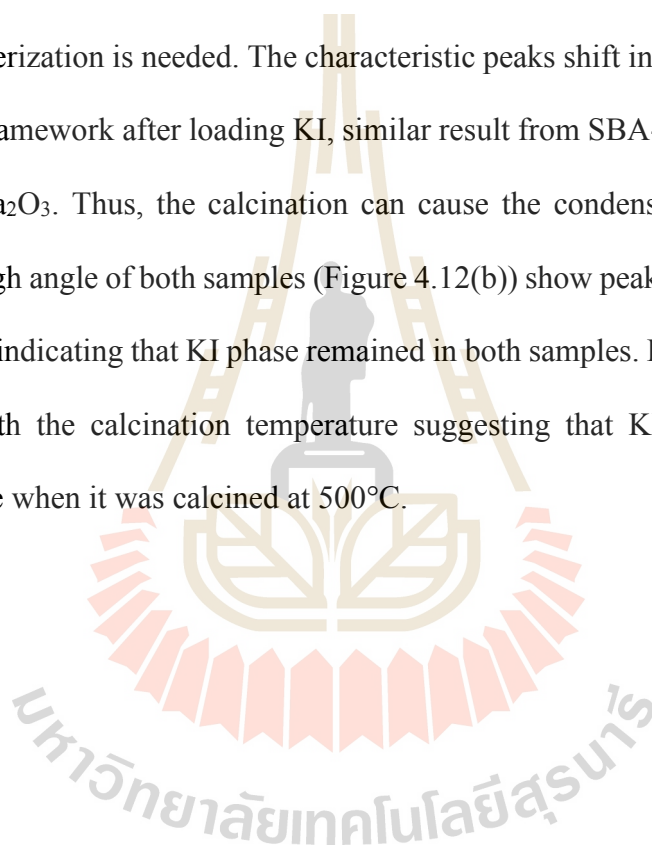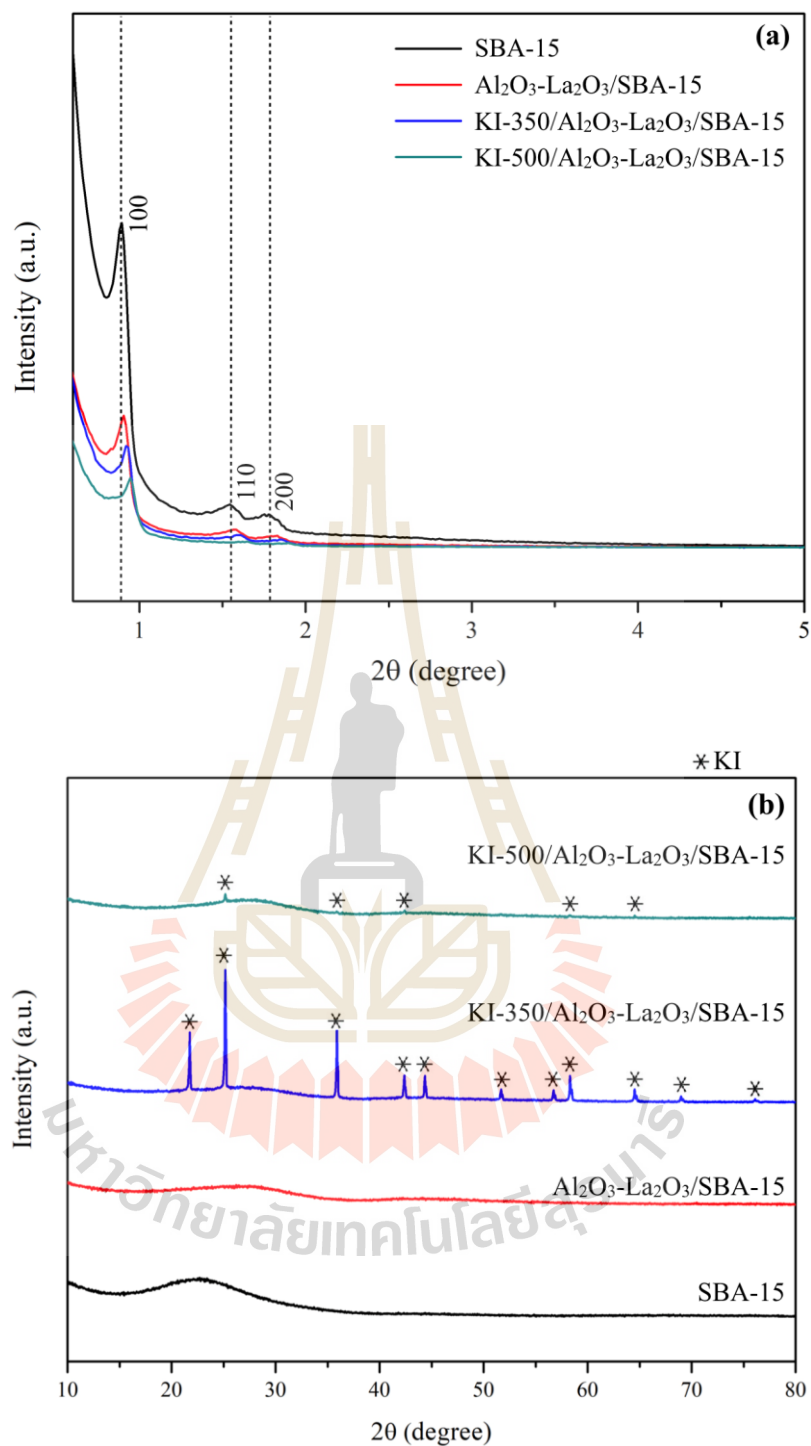
Figure 4.12 XRD patterns at (a) low angle and (b) high angle of SBA-15, Al_2O_3-La_2O_3/SBA-15, KI-350/Al_2O_3-La_2O_3/SBA-15 and KI-500/Al_2O_3-La_2O_3/SBA-15 (KI supported on Al_2O_3-La_2O_3/SBA-15 calcined at 350 and 500°C).

4.2.2 Mesoporous character and surface area

Figure 4.13 shows N_2 adsorption-desorption of SBA-15, Al_2O_3-La_2O_3/SBA-15, KF-350/Al_2O_3-La_2O_3/SBA-15 and KF-500/Al_2O_3-La_2O_3/SBA-15. SBA-15 shows the type IV isotherm with H1 hysteresis lope (see discussion in section 4.1.2). Compared to SBA-15, Al_2O_3-La_2O_3/SBA-15 has smaller adsorbed volume to form monolayer and slightly broader hysteresis loop. The observed hysteresis loop confirms that mesoporous character remains. The broader hysteresis loop implies that Al_2O_3 and La_2O_3 located in the pores of SBA-15. Table 4.3 presents BET surface areas, pore volumes and pore diameters of the samples. The lower monolayer adsorption, surface area and pore volume result from the coverage of SBA-15 surface by loaded Al_2O_3 and La_2O_3. Form KF-350/Al_2O_3-La_2O_3/SBA-15 and KF-500/Al_2O_3-La_2O_3/SBA-15, adsorbed volumes to form a monolayer and their surface area and pore volume (Table 4.3) are very low. Moreover, an absorption and desorption branch overlaps for the sample calcined at 350°C and completely overlaps for the other calcined 500°C. These confirms that these samples do not have mesopores agreed with XRD results. Liu et al. (2017a) have reported that the SBA-15 structure of Al_2O_3-La_2O_3/SBA-15 remained after loading with 7.5wt.% KF. Compared with this work, loading of KF 12wt.% results in completely collapse of SBA-15 structure. Therefore, the degree of collapse of the SBA-15 structure depends on KF loading.
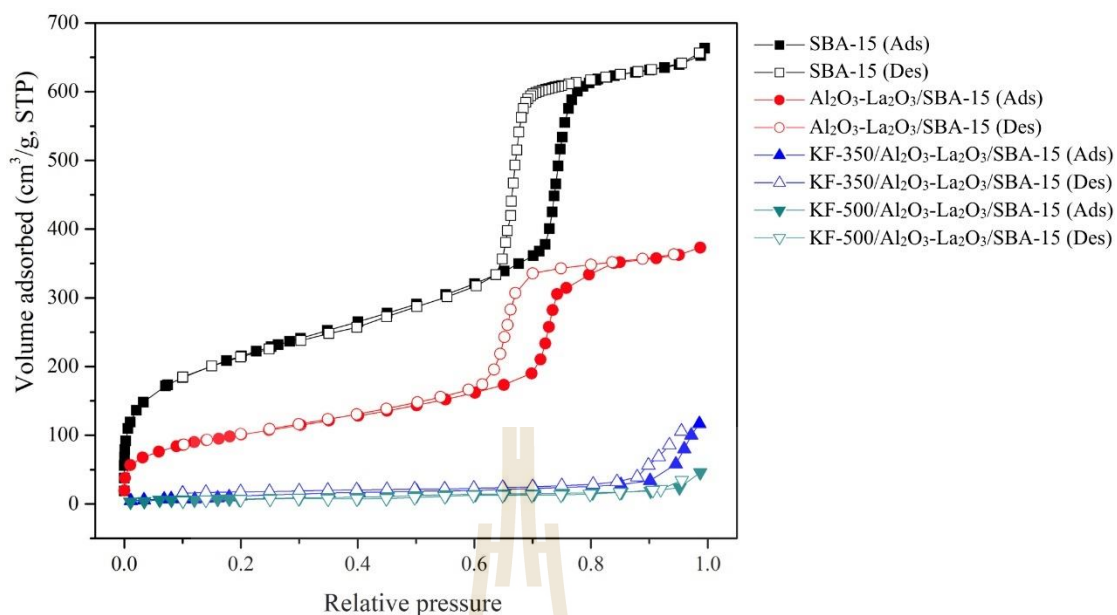
Figure 4.13 N$_2$ adsorption-desorption isotherms of SBA-15, Al$_2$O$_3$-La$_2$O$_3$/SBA-15, KF-350/Al$_2$O$_3$-La$_2$O$_3$/SBA-15 and KF-500/Al$_2$O$_3$-La$_2$O$_3$/SBA-15 (KF supported on Al$_2$O$_3$-La$_2$O$_3$/SBA-15 calcined at 350 and 500°C).

Table 4.3 BET surface areas (S_{BET}), mesopore volume (V_{meso}), micropore volume (V_{micro}), total pore volume (V_{total}) and pore diameters (D_p) of SBA-15, Al_2O_3-La_2O_3/SBA-15, KF-350/Al_2O_3-La_2O_3/SBA-15, KF-500/Al_2O_3-La_2O_3/SBA-15, KI-350/ Al_2O_3-La_2O_3/ SBA-15 and KI-500/Al_2O_3-La_2O_3/SBA-15.

Sample	S_{BET} [a] (m^2/g)	V_{meso} [b] (cm^3/g)	V_{micro} [c] (cm^3/g)	V_{total} (cm^3/g)	D_p [c] (nm)
SBA-15	756	0.94	0.04	0.98	6.2
Al_2O_3-La_2O_3/SBA-15	363	0.57	0.01	0.58	6.0
KF-350/Al_2O_3-La_2O_3/SBA-15	52	0.17	-	0.17	19.7
KF-500/Al_2O_3-La_2O_3/SBA-15	27	0.07	-	0.07	13.4
KI-350/Al_2O_3-La_2O_3/SBA-15	162	0.31	-	0.31	6.5
KI-500/Al_2O_3-La_2O_3/SBA-15	114	0.23	-	0.23	6.8

[a]S_{BET} is surface area calculated by BET equation

[b]V_{meso} is mesopore volume calculated by BJH method from the desorption branch

[c]V_{micro} is micropore volume calculated by t-plot method

[c]D_p is average pore diameter calculated by BJH equation from the desorption branch

Figure 4.14(a) shows N_2 adsorption-desorption of SBA-15, Al_2O_3-La_2O_3/ SBA-15, KI-350/Al_2O_3-La_2O_3/SBA-15 and KI-500/Al_2O_3-La_2O_3/SBA-15. KI-350/ Al_2O_3-La_2O_3/SBA-15 and KI-500/Al_2O_3-La_2O_3/SBA-15 have very low adsorbed volume to form monolayer with observed hysteresis loops. Table 4.3 presents BET surface areas, pore volumes and pore diameters of the samples. A decrease of monolayer adsorption, surface area and pore volume indicate that structure collapse

occurrs. However, the observed hysteresis loops indicate that the mesopores remain. Both samples exhibit short and narrow hysteresis loop attributing to type H5 and the loop is shorter and broader from KI-500/Al_2O_3-La_2O_3/SBA-15. IUPAC technical report (Thommes et al., 2015) explains relation between hysteresis loops and pore characters that type H1 is found in uniform mesopores materials as type H5 is found in partially blocked mesopores. The different hysteresis loop indicates that KI agglomerates in the mesopores of SBA-15 from both samples. The similar results have been reported by Gao et al. (2015) and Das et al. (2018). Moreover, the agglomeration tends to increase with calcination temperature. Therefore, Al_2O_3-La_2O_3/SBA-15 after loading with KI has partially collapsed mesopores with plugging of KI particles.

The pore size distributions of SBA-15, Al_2O_3-La_2O_3/SBA-15, KI-350/Al_2O_3-La_2O_3/SBA-15 and KI-500/Al_2O_3-La_2O_3/SBA-15 are displayed in Figure 4.14(b). The pore distribution of Al_2O_3-La_2O_3/SBA-15 is wider than SBA-15 resulting from a present of Al_2O_3-La_2O_3 in SBA-15 pores, but its pore diameter does not change significantly (Table 4.3). The pore distributions of KI-350/Al_2O_3-La_2O_3/SBA-15 and KI-500/Al_2O_3-La_2O_3/ SBA-15 are broader than Al_2O_3-La_2O_3/SBA-15. This may result from agglomeration of KI in the mesopores. Moreover, the distribution of KI-500/Al_2O_3-La_2O_3/SBA-15 is broader than KI-350/Al_2O_3-La_2O_3/SBA-15 implying more plugging of KI on the mesopores.
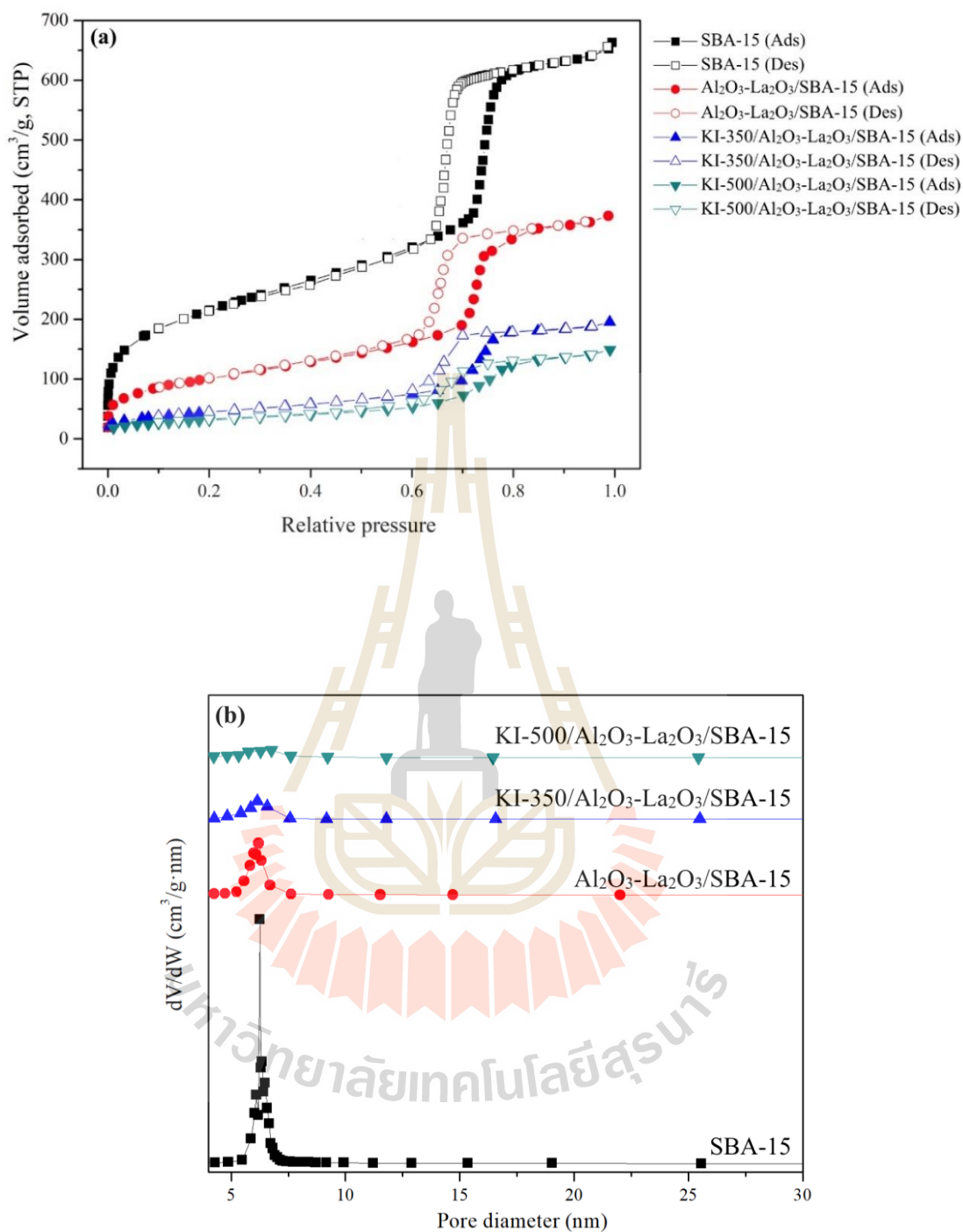
Figure 4.14 N_2 adsorption-desorption isotherms (a) and pore size distributions (b) of

SBA-15, Al_2O_3-La_2O_3/SBA-15, KI-350/Al_2O_3-La_2O_3/SBA-15 and KI-500/Al_2O_3-

La_2O_3/SBA-15 (KI supported on Al_2O_3-La_2O_3/SBA-15 calcined at 350 and 500°C).

4.2.3 SBA-15 framework and functional groups

Figure 4.15 displays FTIR spectra of all samples. SBA-15 spectrum shows the vibration of SBA-15 framework (see detail in section 4.1.3). Al_2O_3-La_2O_3/SBA-15 spectrum shows the vibration of SBA-15 framework without peak of silanol groups assuring that almost of them reacted with loaded Al_2O_3 and La_2O_3 before loading with KF and KI (see more detail in section 4.1.3). Spectra of , KF-350/Al_2O_3-La_2O_3/SBA-15, KF-500/Al_2O_3-La_2O_3/SBA-15, KI-350/Al_2O_3-La_2O_3/SBA-15 and KI-500/Al_2O_3-La_2O_3/SBA-15 are similar to that of Al_2O_3-La_2O_3/SBA-15. KF-350/Al_2O_3-La_2O_3/SBA-15 and KF-500/ Al_2O_3-La_2O_3/ SBA-15 still show the vibration peaks of Si-O-Si and Si-O although the SBA-15 structure collapses.

A broad peak around 3445 cm^{-1} attributing to H_2O stretching (Costa et al., 2016) and more transmittance of H_2O bending at 1636 cm^{-1} are observed form KI-350/Al_2O_3-La_2O_3/SBA-15 and KI-500/Al_2O_3-La_2O_3/SBA-15 implying that KI on Al_2O_3-La_2O_3/SBA-15 could absorb water.
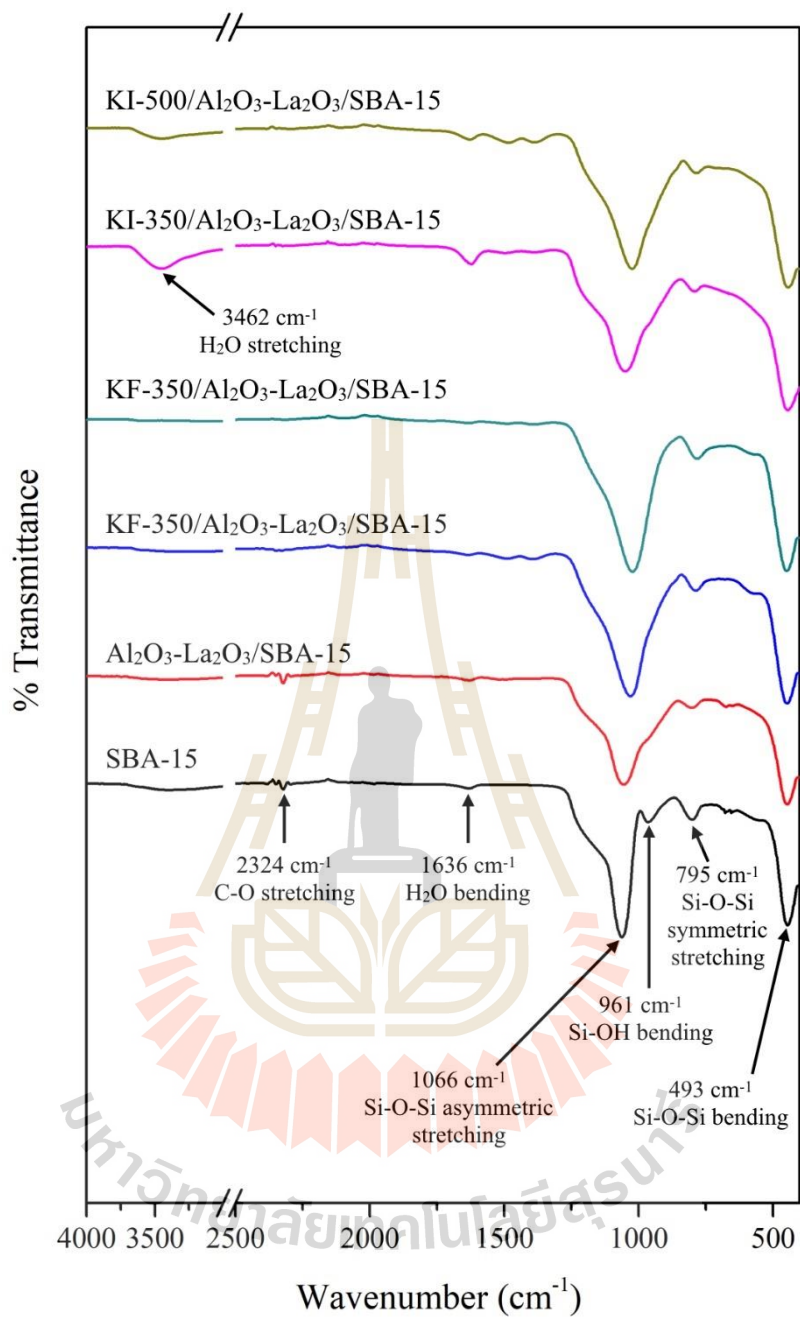
Figure 4.15 FTIR spectra of SBA-15, Al_2O_3-La_2O_3/SBA-15, KF-350/Al_2O_3-La_2O_3/ SBA-15, KF-500/Al_2O_3-La_2O_3/SBA-15, KI-350/Al_2O_3-La_2O_3/SBA-15 and KI-500/ Al_2O_3-La_2O_3/SBA-15.

4.2.4 Identification of phase of loaded potassium

Figure 4.16 displays XANES spectra of standard KF and K_2O, KF-350/Al_2O_3-La_2O_3/SBA-15 and KF-500/Al_2O_3-La_2O_3/SBA-15. The edge energies of standard KF and K_2O and all samples are presented in Table 4.4. Their absorption edges do not shift from that of KF standard (Table 4.4). Therefore, potassium in KF-350/Al_2O_3-La_2O_3/SBA-15 and KF-500/Al_2O_3-La_2O_3/SBA-15 has oxidation state +1. The feature spectra of KF-350/ Al_2O_3-La_2O_3/SBA-15 and KF-500/Al_2O_3-La_2O_3/SBA-15 are similar to that of standard KF indicating that potassium in both samples is in KF phase, similar to that of KF/Al_2O_3/SBA-15. Introduction of La_2O_3 in the support does not give any different in potassium phase.

The peaks of XANES spectra are assigned in these symbols to aid the discussion about KF particle size and interaction with the support: edge energy assigned to A, white line assigned to B and the following peak assigned as C. Compared to the KF standard, peak B (white line) intensity decreases with shift of peak C to lower energy. Kamijo et al. (1996) have reported similar result from $K_2O \cdot nSiO_2$ (n = 2,3,4) glass spectrum when the number of n increased. This suggests that the white line relates to the interaction between potassium and SiO_2. According to this literature, potassium in KF-350/Al_2O_3-La_2O_3/SBA-15 and KF-500/Al_2O_3-La_2O_3/SBA-15 may have a strong interaction with support. Sun et al. (2015) have also proposed that the strong interaction between loaded metal and SBA-15 is a main reason in causing a collapse of SBA-15. By comparison, the white line of KF/Al_2O_3/SBA-15 does not decrease (see section 4.1.4) suggesting that the interaction between KF and Al_2O_3/SBA-15 is lower than KF on Al_2O_3-La_2O_3/SBA-15.
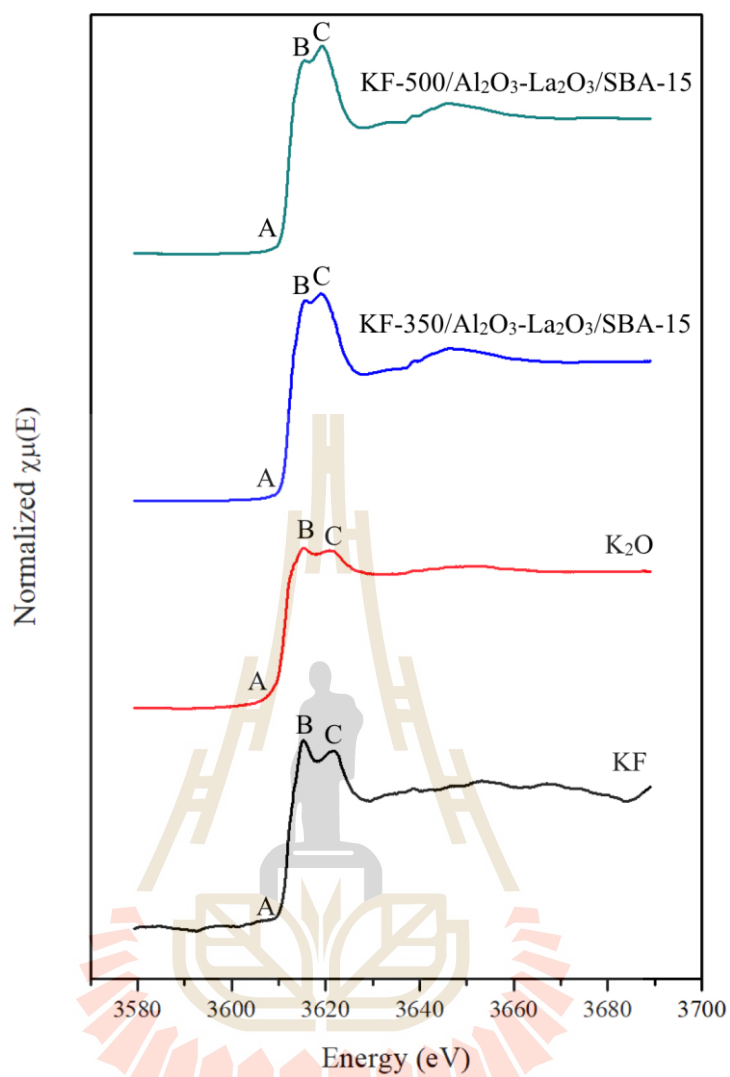
Figure 4.16 XANES spectra of standard KF and K_2O, KF-350/Al_2O_3-La_2O_3/SBA-15 and KF-500/Al_2O_3-La_2O_3/SBA-15 (KF supported on Al_2O_3-La_2O_3 calcined at 350 and 500°C).

Table 4.4 The absorption edge energies of standard KF, KI and K_2O and SBA-15, Al_2O_3-La_2O_3/SBA-15, KF-350/Al_2O_3-La_2O_3/SBA-15, KF-500/Al_2O_3-La_2O_3/SBA-15, KI-350/ Al_2O_3-La_2O_3/ SBA-15 and KI-500/Al_2O_3-La_2O_3/SBA-15.

Sample	Edge energy (eV)
KF	3612.0
KI	3612.7
K_2O	3611.7
KF-350/Al_2O_3-La_2O_3/SBA-15	3612.5
KF-500/Al_2O_3-La_2O_3/SBA-15	3612.2
KI-350/Al_2O_3-La_2O_3/SBA-15	3612.3
KI-500/Al_2O_3-La_2O_3/SBA-15	3612.2

Figure 4.17 shows XANES spectra of standard KI and K_2O, KI-350/Al_2O_3-La_2O_3/SBA-15 and KI-500/Al_2O_3-La_2O_3/SBA-15. The oxidation states of potassium in KI-350/Al_2O_3-La_2O_3/SBA-15 and KI-500/Al_2O_3-La_2O_3/SBA-15 are +1 confirming from similar energy edge of samples to that of potassium standards (Table 4.4). However, the feature spectra of KI-350/Al_2O_3-La_2O_3/SBA-15 and KI-500/Al_2O_3-La_2O_3/SBA-15 is different. The feature spectrum of KI-350/Al_2O_3-La_2O_3/SBA-15 has the combination of standard KI and K_2O features suggesting that potassium phase in this sample is the mixed phase of KI and K_2O phase. The feature spectrum of KI-500/Al_2O_3-La_2O_3/SBA-15 has similar feature of K_2O with slightly feature of KI, similar to that of KI/Al_2O_3/SBA-15. Therefore, potassium in KI-500/Al_2O_3-La_2O_3/SBA-15 is

in K_2O as major phase and KI as minor phase. Thus, KI on Al_2O_3-La_2O_3/SBA-15 tends

to convert from KI to K_2O when increasing of calcination temperature.
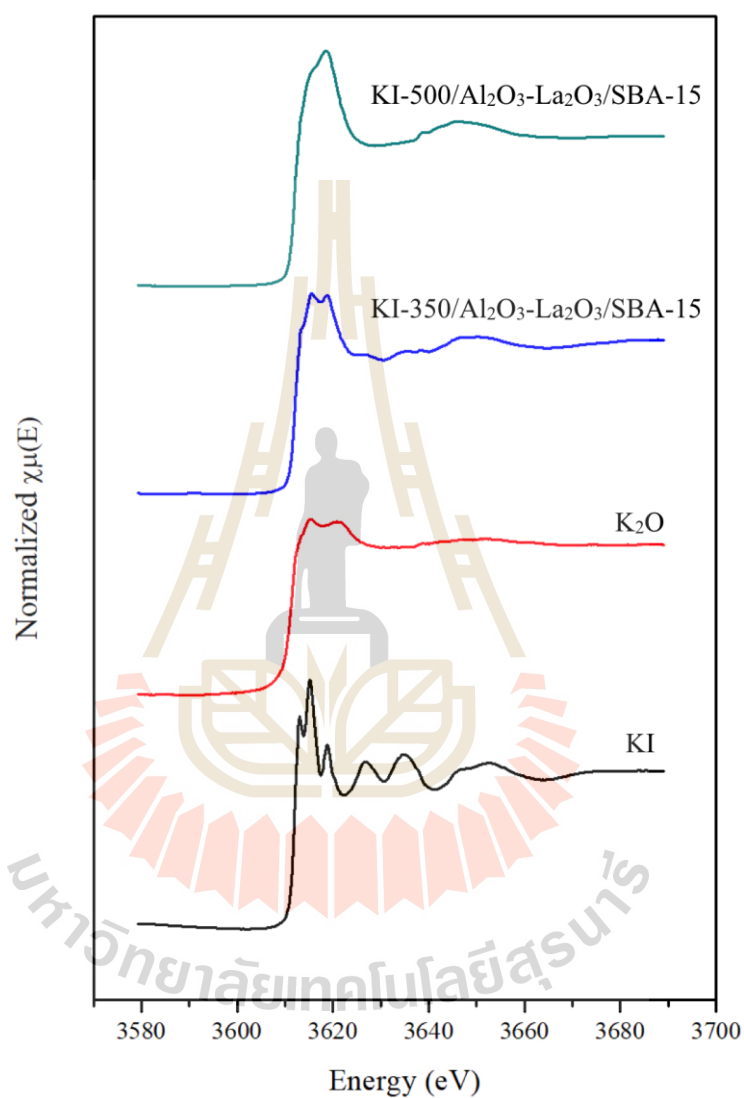
Figure 4.17 XANES spectra of standard KI and K_2O, KI-350/Al_2O_3-La_2O_3/SBA-15

and KI-500/Al_2O_3-La_2O_3/SBA-15 (KI supported on Al_2O_3-La_2O_3 calcined at 350 and

500°C).

4.2.5 Study of base property

Figure 4.18 shows conversion of MBOH over SBA-15, Al_2O_3-La_2O_3/SBA-15, KF-350/ Al_2O_3-La_2O_3/SBA-15 and KF-500/Al_2O_3-La_2O_3/SBA-15. The conversion and products over SBA-15 are already discussed in section 4.1.5. After loading with Al_2O_3-La_2O_3, the conversion of MBOH is almost 100% over Al_2O_3-La_2O_3/SBA-15 at the begininng of reaction, and then drops with time on stream indicating that the material deactivates over time on stream. The conversion of MBOH over KF-350/Al_2O_3-La_2O_3/SBA-15 reaches 52% even through the surface area only 52 m^2/g. The catalytic activity remarkably decreases to 18% for KF-500/Al_2O_3-La_2O_3/SBA-15 resulting from decrease of its surface area.
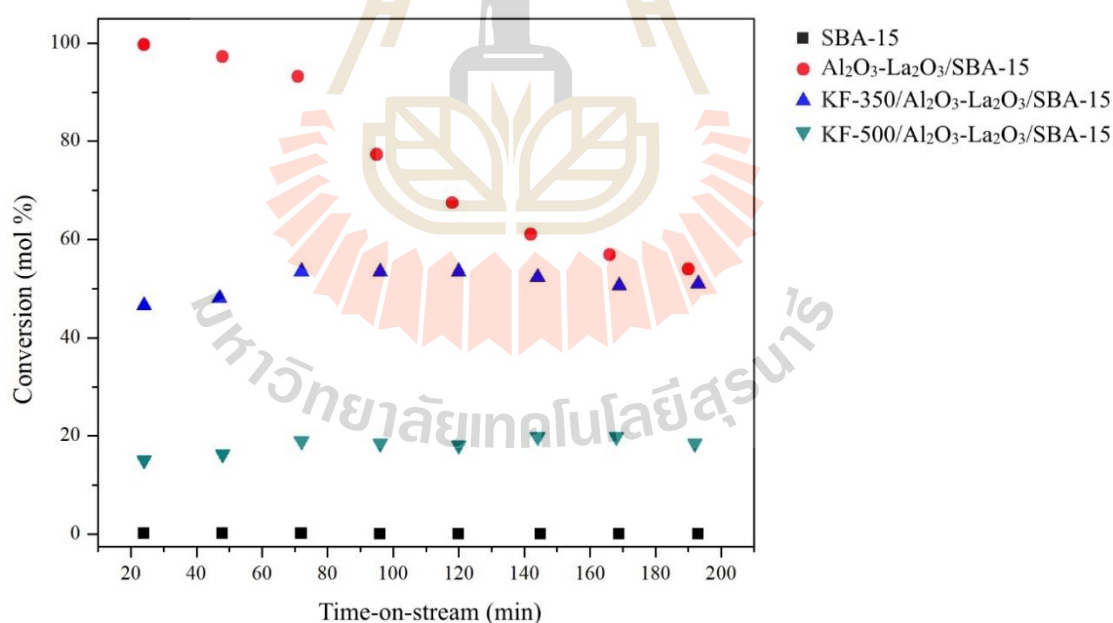
Figure 4.18 Conversion of MBOH over SBA-15, Al_2O_3-La_2O_3/SBA-15, KF-350/Al_2O_3-La_2O_3/SBA-15 and KF-500/Al_2O_3-La_2O_3/SBA-15, reaction temperature 150°C.

Acetylene and acetone selectivity of SBA-15, Al_2O_3-La_2O_3/SBA-15, KF-350/ Al_2O_3-La_2O_3/SBA-15 and KF-500/Al_2O_3-La_2O_3/SBA-15 are shown in Figure 4.19 and 4.20, respectively. The main product from Al_2O_3-La_2O_3/SBA-15 was MBYNE from acid pathway and minor products are acetylene and acetone from base pathway. This result indicates that Al_2O_3-La_2O_3/SBA-15 contains both acid and base sites. Compared to Al_2O_3/SBA-15, the addition of La_2O_3 provides base sites in materials. At 20 minutes on stream, acetone is not observed resulting from the consecutive consumption through aldol condensations and Michael addition reaction (Cosimo and Apesteguía, 1998; Aramendia et al., 1999)

The products of both KF-350/Al_2O_3-La_2O_3/SBA-15 and KF-500/Al_2O_3-La_2O_3/SBA-15 were acetylene and acetone confirming base property of materials. The molar ratio of them are 0.9 for both samples slightly deviating from one, the theroritical value, resulting from consuming of acetone by the mentioned reason. The catalytic activity of KF on Al_2O_3-La_2O_3/SBA-15 significantly improves compared with KF on Al_2O_3/SBA-15. Hence, La_2O_3 enhances base property of material, agree with the work of Liu et al. (2017b). However, the collapse of SBA-15 structure leads to the decrease of their catalytic activity.
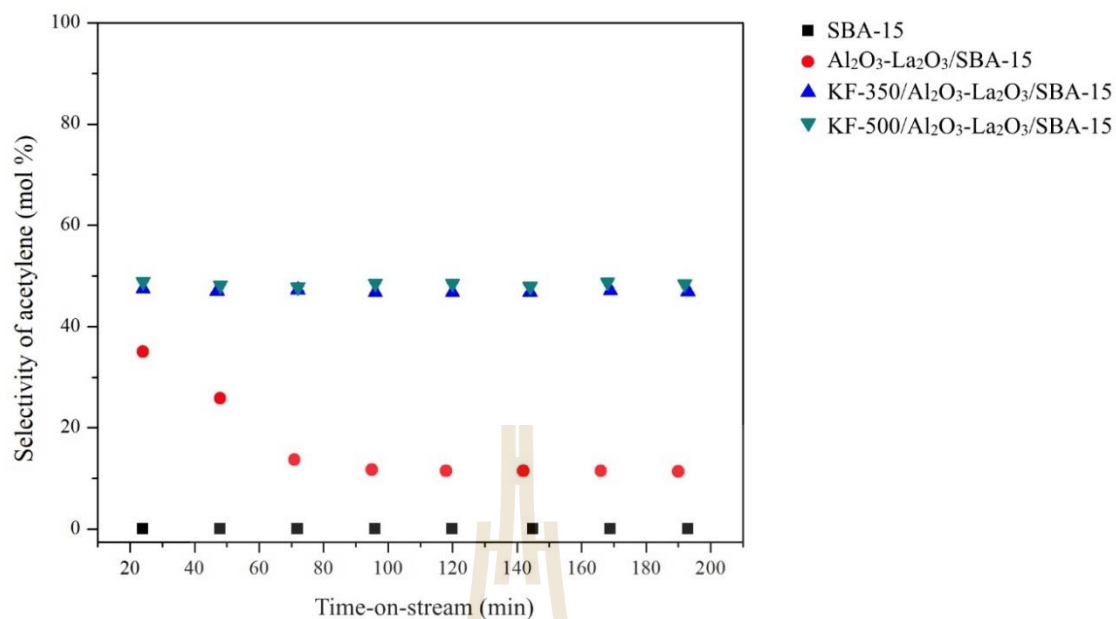
Figure 4.19 Selectivity of acetylene over SBA-15, Al_2O_3-La_2O_3/SBA-15, KF-350/Al_2O_3-La_2O_3/SBA-15 and KF-500/Al_2O_3-La_2O_3/SBA-15, reaction temperature 150°C.
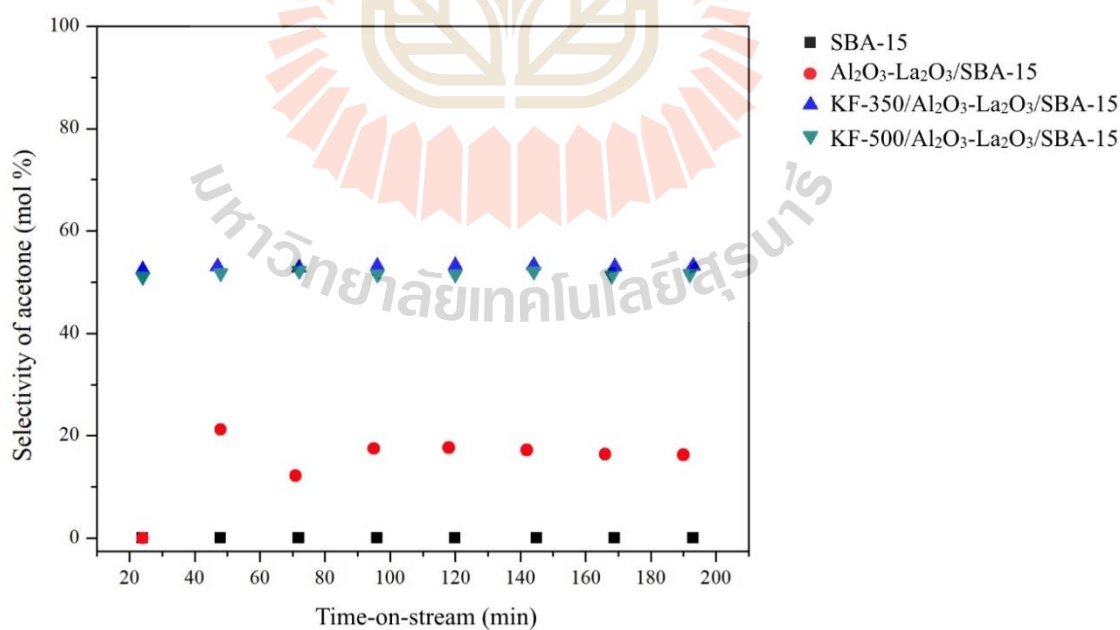
Figure 4.20 Selectivity of acetone over SBA-15, Al_2O_3-La_2O_3/SBA-15, KF-350/Al_2O_3-La_2O_3/SBA-15 and KF-500/Al_2O_3-La_2O_3/SBA-15, reaction temperature 150°C.

Figure 4.21 shows conversion of MBOH over SBA-15, Al$_2$O$_3$-La$_2$O$_3$/SBA-15, KI-350/ Al$_2$O$_3$-La$_2$O$_3$/SBA-15 and KI-500/Al$_2$O$_3$-La$_2$O$_3$/SBA-15. The conversion over KI-350/Al$_2$O$_3$-La$_2$O$_3$/SBA-15 is 97-98% over 190 minutes on stream. The conversion over KI-500/Al$_2$O$_3$-La$_2$O$_3$/SBA-15 is almost 100% at the beginnig of reaction, and drops at 60 miniutes on stream indicating that the sample deactivates.
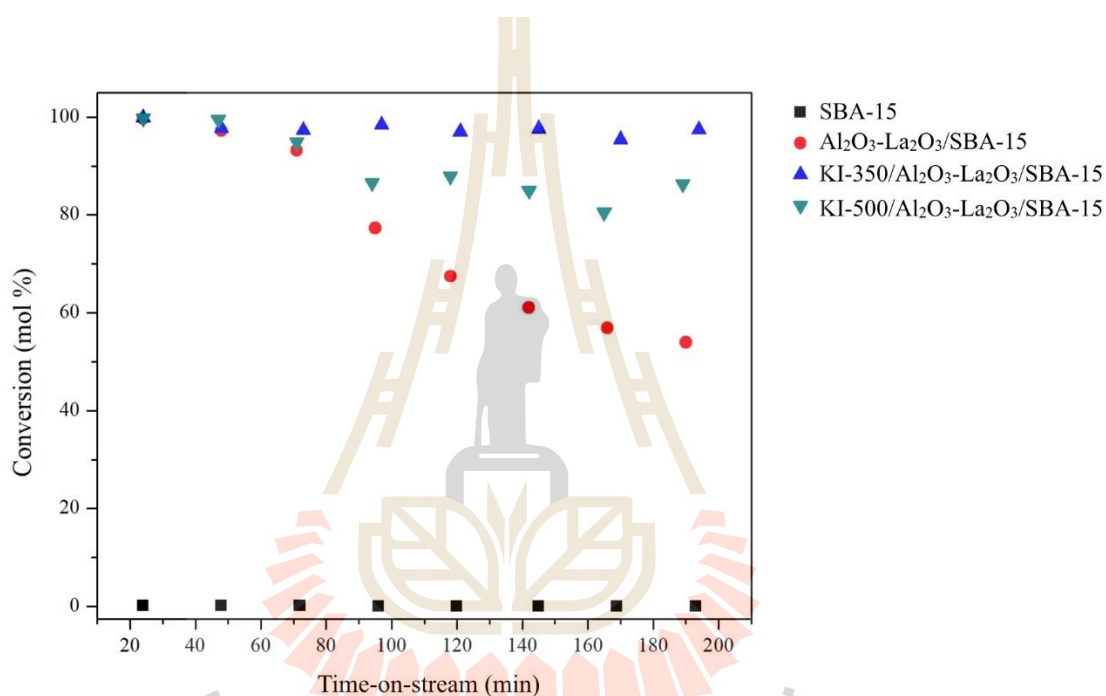
Figure 21 Conversion of MBOH over SBA-15, Al$_2$O$_3$-La$_2$O$_3$/SBA-15, KI-350/Al$_2$O$_3$-La$_2$O$_3$/SBA-15 and KI-500/Al$_2$O$_3$-La$_2$O$_3$/SBA-15, reaction temperature 150°C.

The selectity of acetylene and acetone of SBA-15, Al_2O_3-La_2O_3/SBA-15, KI-350/ Al_2O_3-La_2O_3/SBA-15 and KI-500/Al_2O_3-La_2O_3/SBA-15 are shown in Figure 4.22 and 4.23, respectively. The obtained products from KI-350/Al_2O_3-La_2O_3/SBA-15 and KI-500/Al_2O_3-La_2O_3/SBA-15 were acetylene and acetone. Thier molar ratio from both samples are 0.9, slightly deviating from one due to consumption of acetone. Thus, both of KI-350/Al_2O_3-La_2O_3/SBA-15 and KI-500/Al_2O_3-La_2O_3/SBA-15 possess base sites.
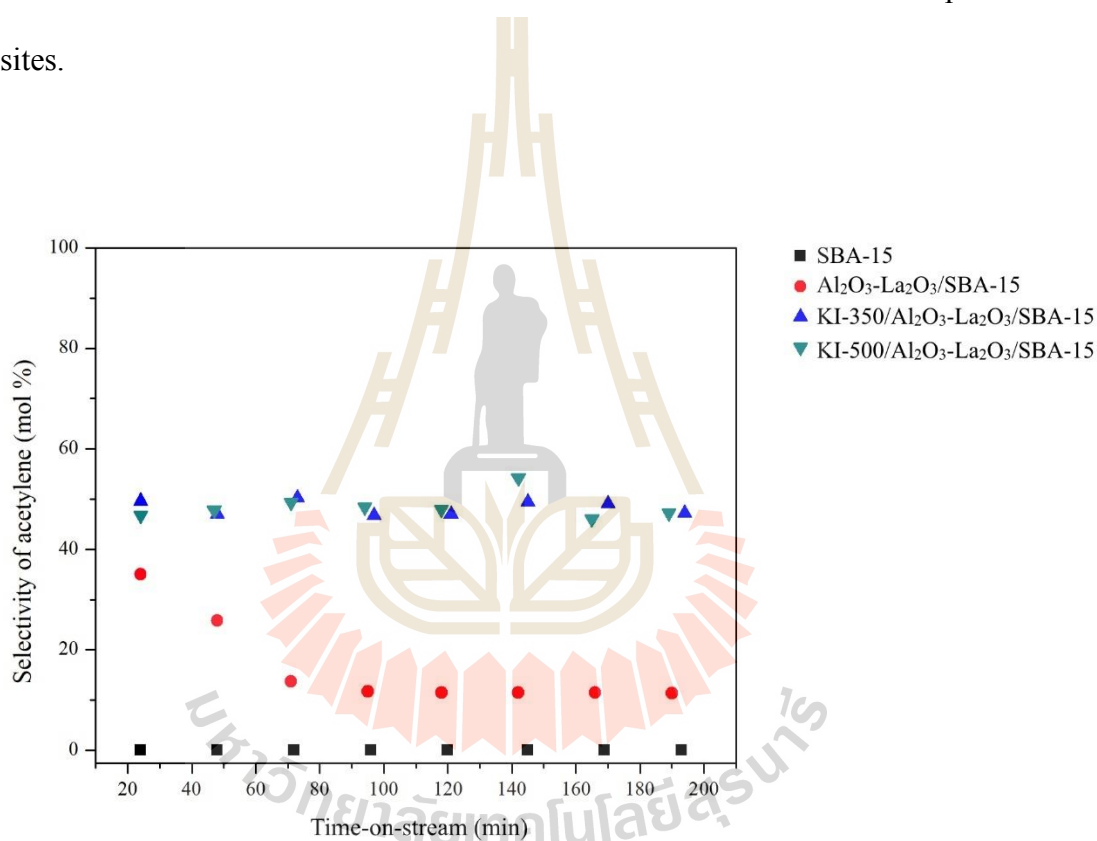
Figure 4.22 Selectivity of acetylene over SBA-15, Al_2O_3-La_2O_3/SBA-15, KI-350/ Al_2O_3-La_2O_3/SBA-15 and KI-500/Al_2O_3-La_2O_3/SBA-15, reaction temperature 150°C.
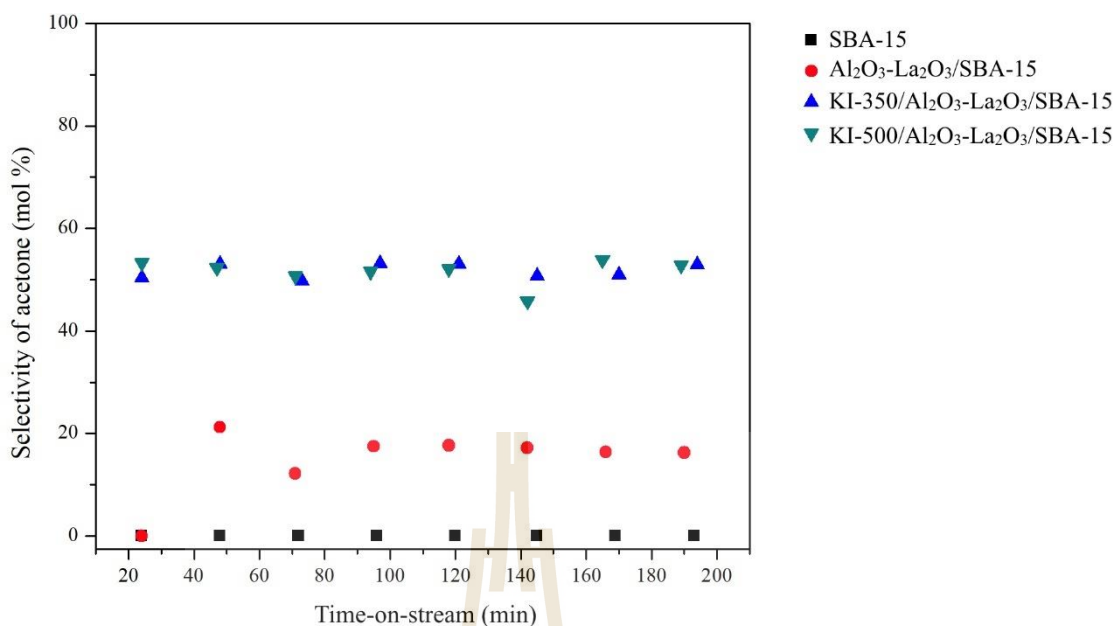
Figure 4.23 Selectivity of acetone over SBA-15, Al_2O_3-La_2O_3/SBA-15, KI-350/Al_2O_3-La_2O_3/SBA-15 and KI-500/Al_2O_3-La_2O_3/SBA-15, reaction temperature 150°C.

Nonetheless, the deactivation of KI-500/Al_2O_3-La_2O_3/SBA-15 is worth a discussion. Huang and Kaliaguine (1993) tested MBOH conversion on alkali-exchanged zeolites to study Lewis acid-base property. Zeolites after adsorprion of MBOH followed by heating to the reatction temperature were studied by FTIR. The adsored species were residual MBOH, acetone and diacetone alcohol produced from aldol condensation of acetone. The relationiship between C=O infrared band intensity corresponding to adsored acetone and the negative charge of framework oxygen was studied. The higher negative charge of oxygen resulted in the stronger intensity of C=O band. The higher amount of adsored species also related to more deactivation of zeolite on MBOH conversion. Thus, deactivation of zeolite causes from adsorption of MBOH, aceone and condensed acetone product. From these data, the deactivation of KI-

500/Al$_2$O$_3$-La$_2$O$_3$/SBA-15 may result from the adsorption of residual MBOH, acetone and diacetone alcohol. XANES results indicates that KI on Al$_2$O$_3$-La$_2$O$_3$/SBA-15 calcined at 500°C has the distribution of K$_2$O phase better than the sample calcined at 350°C. Thus, KI-500/Al$_2$O$_3$-La$_2$O$_3$/SBA-15 has higher negative charge from the oxygen of K$_2$O. Consequently, KI on Al$_2$O$_3$-La$_2$O$_3$/SBA-15 calcined at 500°C deactivates at 70 minutes on stream whereas the catalytic activity is steady over 190 minutes on stream for the sample calcined at 350°C.

4.3 Catalytic performance on transesterification

The synthesized materials were tested in transesterification with glyceryl trioctanoate and methanol. Glyceryl triocatanoate was applied as a reactant instead of plant oils to avoid conversion from other components in oils.

%FAME yield over SBA-15, Al$_2$O$_3$/SBA-15, KF/Al$_2$O$_3$/SBA-15 and KI/Al$_2$O$_3$/SBA-15 are shown in Figure 4.24. SBA-15 and Al$_2$O$_3$/SBA-15 did not give any FAME because SBA-15 does not contain any acid or base sites and Al$_2$O$_3$/SBA-15 has only acid sites which could produce low methyl ester. KF/Al$_2$O$_3$/SBA-15 and KI/Al$_2$O$_3$/SBA-15 gave a small amount of FAME. Their catalytic performances agree with the study of MBOH conversion that KF/Al$_2$O$_3$/SBA-15 and KI/Al$_2$O$_3$/SBA-15 contain low base sites resulting in low %FAME produced.
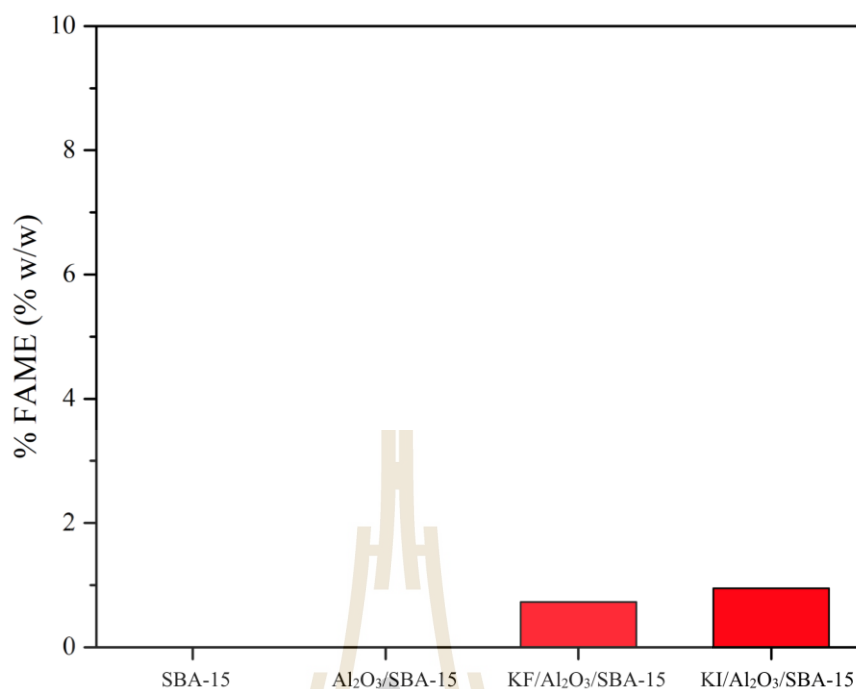
Figure 4.24 %FAME in the product from SBA-15, Al_2O_3/SBA-15, KF/Al_2O_3/SBA-15 and KI/Al_2O_3/SBA-15 calcined at 500°C.

The amounts of %FAME from SBA-15, Al_2O_3-La_2O_3/SBA-15, KF-350/Al_2O_3-La_2O_3/SBA-15, KF-500/Al_2O_3-La_2O_3/SBA-15, KI-350/Al_2O_3-La_2O_3/SBA-15 and KI-500/Al_2O_3-La_2O_3/SBA-15 are shown in Figure 4.25. Al_2O_3-La_2O_3/SBA-15 did not produce any methyl ester. K on Al_2O_3-La_2O_3/SBA-15 produced small amount of methyl ester. Nonetheless, 10%w/w methyl ester was produced from KF-500/Al_2O_3-La_2O_3/SBA-15. From overall catalytic performance, the studied materials are not active in transesterification although they possess base sites confirmed by MBOH conversion testing. Compared to the results reported by Rakmae et al. (2016), the results from this work are remarkably low. The catalysts were further characterized by XPS technique to investigate the reason.
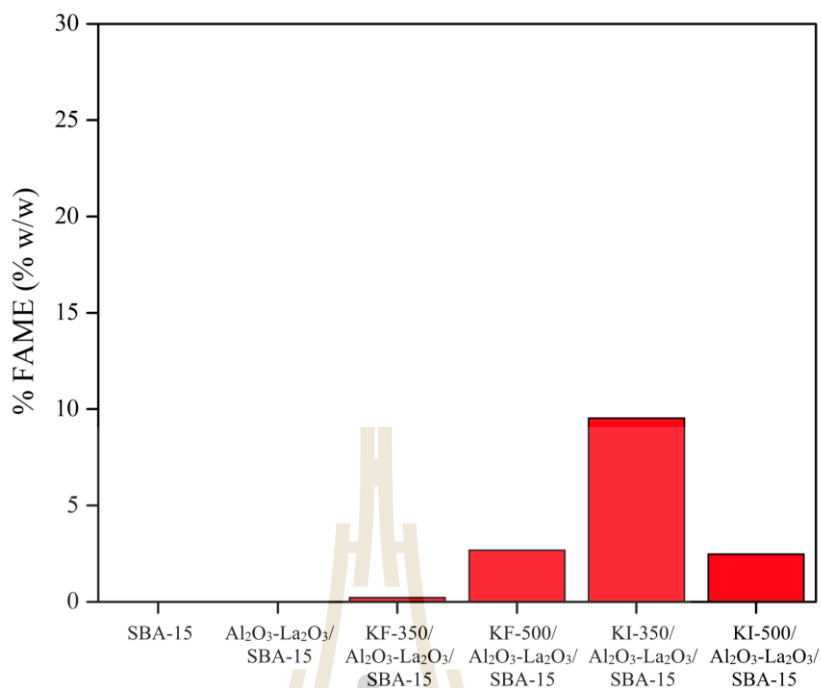
Figure 4.25 %FAME in the product from SBA-15, SBA-15, KF-350/Al$_2$O$_3$-La$_2$O$_3$/SBA-15 and KI-350/Al$_2$O$_3$-La$_2$O$_3$/SBA-15 calcined at 350°C and KF-500/Al$_2$O$_3$-La$_2$O$_3$/SBA-15 and KI-500/Al$_2$O$_3$-La$_2$O$_3$/SBA-15 calcined at 500°C.

Figure 4.26 displays XPS spectrum of La 3d region of KI-350/Al$_2$O$_3$-La$_2$O$_3$/SBA-15. The binding energies are 836.4 eV for La 3d$_{5/2}$ and 853.4 eV for of La 3d$_{3/2}$. La 3d$_{5/2}$ and La 3d$_{3/2}$ correspond to spin orbital coupling. Its strong interaction causes the splitting of the peaks (Mack, 2019). The different of splitting peaks of La 3d$_{5/2}$ is 3.5 eV which corresponds to lanthanum carbonate (La$_2$(CO$_3$)$_3$) instead of lanthanum oxide (La$_2$O$_3$), the expected phase (Mack, 2019).

The most sensible explanation is that La$_2$O$_3$ adsorbed CO$_2$, and therefore La$_2$O$_3$ at surface changed to La$_2$(CO$_3$)$_3$ form. For transesterification testing, the catalysts were dried at 120°C before reaction and the reaction was operated under air atmosphere.

Whereas MBOH conversion testing, the materials were activated by heating up to 350°C under N_2 atmosphere, and then kept in this atmosphere until the start of reaction. Base sites from La_2O_3 recovered when absorbed CO_2 was removed from surfaces. Hence, the materials can convert MBOH in MBOH conversion testing but are not active in transesterification.
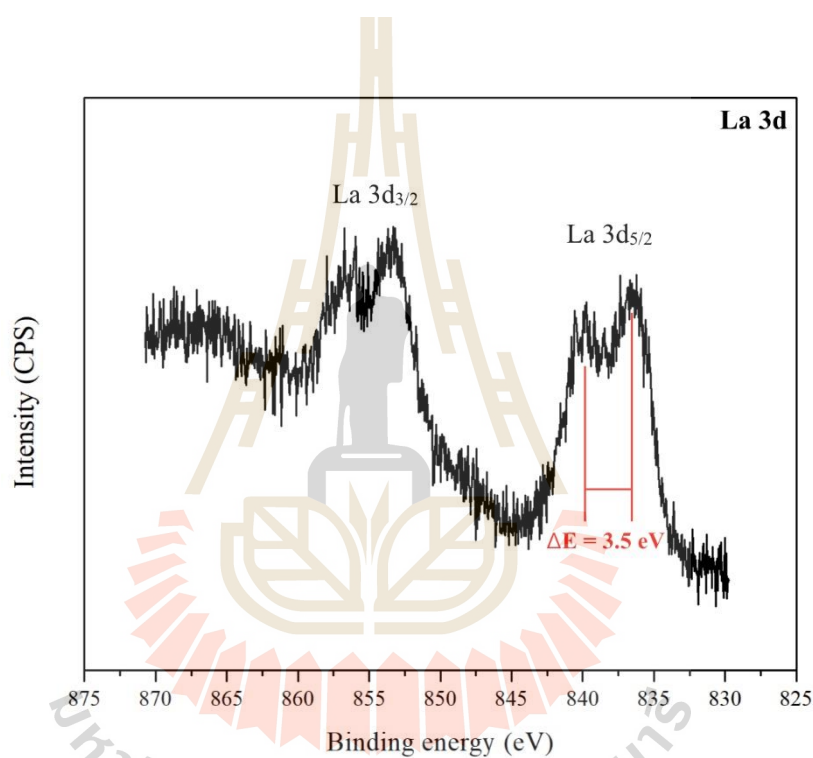
Figure 4.26 XPS spectrum of La 3d orbital.

CHAPTER V

CONCLUSIONS

In this thesis, the base properties of KF and KI on Al_2O_3/SBA-15 and Al_2O_3-La_2O_3/SBA-15 are studied by MBOH catalytic conversion. Al_2O_3/SBA-15 still contains mesoporous character. After Al_2O_3/SBA-15 loaded with potassium precursor and calcined at 500°C, the structure and mesoporous character of SBA-15 are destroyed for KF/Al_2O_3/ SBA-15. Conversely, KI/Al_2O_3/SBA-15 retains the mesoporous character with partial collapse of the structure. Potassium of KF/Al_2O_3/SBA-15 is in KF phase. From KI/Al_2O_3/SBA-15, potassium is in the mixed phase with K_2O as the major phase and KI as the minor phase. Both KF/Al_2O_3/SBA-15 and KI/Al_2O_3/SBA-15 contains basic sites confirmed by products of MBOH conversion. Moreover, KI/Al_2O_3/SBA-15 has slightly higher basicity than KF/Al_2O_3/SBA-15 with MBOH conversion of 20%.

SBA-15 is loaded with Al_2O_3 and La_2O_3 with the same method. Al_2O_3-La_2O_3/SBA-15 retains both the structure and mesopores of SBA-15. After loading with KF and KI, the as-synthesized materials are calcined at 350 and 500°C. KF on Al_2O_3-La_2O_3/ SBA-15 results in severe collapse of SBA-15 structure with extremely low surface area. Moreover, the structure of KF on Al_2O_3-La_2O_3/ SBA-15 calcined at 500°C collapses more than when calcination at 350°C. KI on Al_2O_3-La_2O_3/SBA-15 retains mesoporous character with partial collapse of the structure and plugging of the pores with loaded KI. This more occurs when the calcination temperature increases from 350 to 500°C. Potassium is in KF phase for both KF-350/Al_2O_3-La_2O_3/SBA-15 and KF-500

Al_2O_3-La_2O_3/SBA-15. KF on Al_2O_3-La_2O_3/ SBA-15 has more interaction than that on Al_2O_3/SBA-15. Potassium in KI-350/Al_2O_3-La_2O_3/SBA-15 is in a mixed phase of KI and K_2O. KI converts to K_2O more for KI-500/Al_2O_3-La_2O_3/SBA-15, resulting in K_2O as the major phase and KI as the minor phase.

KF and KI on Al_2O_3-La_2O_3/SBA-15 contain base sites confirmed by MBOH conversion. KF-350/Al_2O_3-La_2O_3/SBA-15 provides 50% conversion of MBOH. The conversion decreases to 18% from KI-500/Al_2O_3-La_2O_3/SBA-15 due to a decrease of the surface area. KI-350/Al_2O_3-La_2O_3/SBA-15 achieves 97.5% MBOH conversion over 190 min on stream with steady catalytic activity. KI-500/Al_2O_3-La_2O_3/SBA-15 deactivates after 60 min on stream. Deactivation of KI-500/Al_2O_3-La_2O_3/SBA-15 may result from adsorption of residual MBOH, acetone and its condensed products by K_2O. KI-500/Al_2O_3-La_2O_3/SBA-15 has more partition of K_2O than KI-350/Al_2O_3-La_2O_3/SBA-15, resulting in deactivation being observed, while KI-350/Al_2O_3-La_2O_3/SBA-15 has steady catalytic activity over 190 min on stream. From the results, basicity of KF and KI on Al_2O_3-La_2O_3/SBA-15 are remarkably higher than on Al_2O_3/SBA-15. Therefore, La_2O_3 introduction on the support significantly improves the basicity of KF/Al_2O_3/SBA-15 and KI/Al_2O_3/SBA-15.

All prepared materials are tested in transesterification with glyceryl trioctanoate and methanol as reactants. All materials are not active for this reaction. K/Al_2O_3/SBA-15 has low basicity, resulting in low catalytic performance. K/Al_2O_3-La_2O_3/SBA-15 has high basicity. However, the XPS result indicates that La is in form La_2O_3 instead of $La_2(CO_3)_3$. This may be the reason for the low catalytic performance in transesterification of K/Al_2O_3-La_2O_3/SBA-15.

REFERENCES
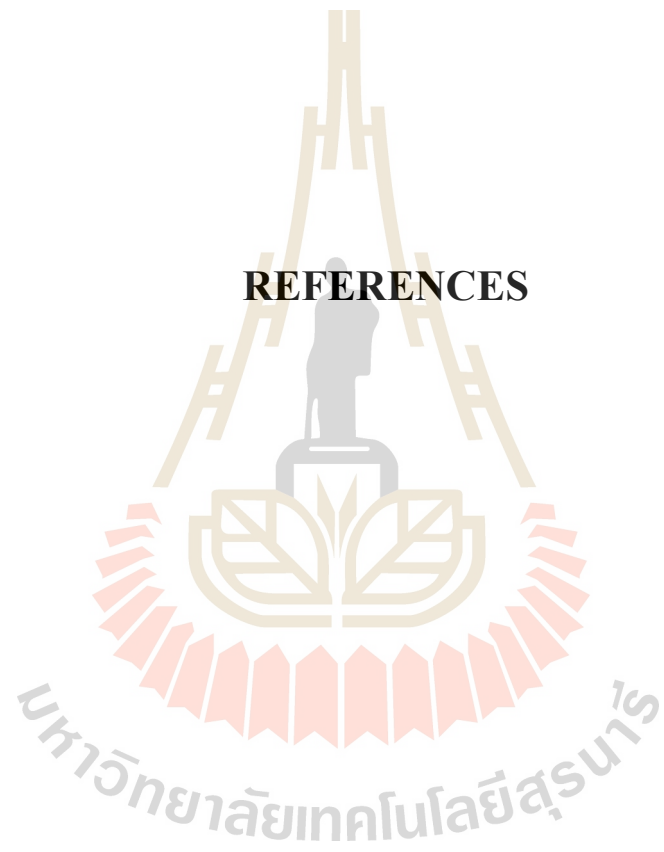
REFERENCES

Alothman, Z. A. (2012). A review: Fundamental aspects of silicate mesoporous materials. **Materials**. 5(12): 2874–2902.

Alsawalha, M. (2004). **Characterization of acidic and basic properties of heterogeneous catalysts by test reactions**. Ph.D. Dissertation, Carl von Ossietzky Universität Oldenburg, Germany.

Aramendía, M. A., Boráu, V., García, I. M., Jiménez, C., Marinas, A., Marinas, J. M., Porras, A. and Urbano, F. J. (1999). Comparison of different organic test reactions over acid-base catalysts. **Applied Catalysis A: General**. 184(1): 115–125.

Baerlocher, Ch. and McCusker L. B. (2007). **Framework type FAU** [On-line]. Available: https://asia.iza-structure.org/IZA-SC/framework.php?STC=FAU

Bertoluzza, A., Fagnano, C., Antonietta Morelli, M., Gottardi, V. and Guglielmi, M. (1982). Raman and infrared spectra on silica gel evolving toward glass. **Journal of Non-Crystalline Solids**. 48(1): 117–128.

Clacens, J.-M., Genuit, D., Delmotte, L., Garcia-Ruiz, A., Bergeret, G., Montiel, R., Lopez, J. and Figueras, F. (2004). Effect of the support on the basic and catalytic properties of KF. **Journal of Catalysis**. 221: 483–490.

Dalla Costa, B. O., Legnoverde, M. S., Lago, C., Decolatti, H. P. and Querini, C. A. (2016). Sulfonic functionalized SBA-15 catalysts in the gas phase glycerol dehydration. Thermal stability and catalyst deactivation. **Microporous and Mesoporous materials**. 230: 66–75.

Das, S., Sengupta, M., Bag, A., Shah, M. and Bordoloi, A. (2018). Facile synthesis of highly disperse Ni-Co nanoparticles over mesoporous silica for enhanced methane dry reforming. **Nanoscale**. 10: 6409–6425.

Decottignies, M., Phalippou, J. and Zarzycki, J. (1978). Synthesis of glasses by hot-pressing of gels. **Journal of Materials Science**. 13(12): 2605–2618.

De Saint Laumer, J. Y., Cicchetti, E., Merle, P., Egger, J. and Chaintreau, A. (2010). Quantification in gas chromatography: Prediction of flame ionization detector response factors from combustion enthalpies and molecular structures. **Analytical Chemistry**. 82(15): 6457–6462.

Di Cosimo, J. I. and Apesteguía, C. R. (1998). Study of the catalyst deactivation in the base-catalyzed oligomerization of acetone. **Journal of Molecular Catalysis A: Chemical**. 130(1–2): 177–185.

Gao, D., Duan, A., Zhang, X., Zhao, Z., E, H., Li, J. and Wang, H. (2015). Synthesis of NiMo catalysts supported on mesoporous Al-SBA-15 with different morphologies and their catalytic performance of DBT HDS. **Applied Catalysis B: Environmental**. 165: 269–284.

Handa, H., Baba, T., Sugisawa, H. and Ono, Y. (1998). Highly efficient self-condensation of benzaldehyde to benzyl benzoate over KF-loaded alumina. **Journal of Molecular Catalysis A: Chemical**. 134(1–3): 171–177.

Harrison, K. (2007). **Triglyceride (Molecule of the Month for March 2007)** [On-line]. Available: http://www.3dchem.com/Triglyceride.asp

Huang, M. and Kaliaguine, S. (1993). Reactions of methylbutynol on alkali-exchanged zeolites. A Lewis acid-base selectivity study. **Catalysis Letters**. 18(4): 373–389.

Ilkiliç, C., Aydin, S., Behcet, R. and Aydin, H. (2011). Biodiesel from safflower oil and its application in a diesel engine. **Fuel Processing Technology**. 92(3): 356–362.

Jacobs, G., Pendyala, V. R. R., Martinelli, M., Shafer, W. D., Gnanamani, M. K., Khalid, S., MacLennan, A., Hu, Y. and Davis, B. H. (2017). Fischer–Tropsch Synthesis: XANES spectra of potassium in promoted precipitated iron catalysts as a function of time on-stream. **Catalysis Letters**. 147(8): 1861–1870.

Kamijo, N., Handa, K. and Umesaki, N. (1996). Soft X-ray XAFS studies on the local structure of K_2O-SiO_2 glasses. **Materials Transactions**. 37(4): 927–931.

Knothe, G. and Razon, L. F. (2017). Biodiesel fuels. **Progress in Energy and Combustion Science**. 58: 36–59.

Kuśtrowski, P., Chmielarz, L., Bozek, E., Sawalha, M. and Roessner, F. (2004). Acidity and basicity of hydrotalcite derived mixed Mg-Al oxides studied by test reaction of MBOH conversion and temperature programmed desorption of NH_3 and CO_2. **Materials Research Bulletin**. 39: 263–281.

Lauron-Pernot, H., Luck, F. and Popa, J. M. (1991). Methylbutynol: a new and simple diagnostic tool for acidic and basic sites of solids. **Applied Catalysis**. 78(2): 213–225.

Lee, A. F., Bennett, J. A., Manayil, J. C. and Wilson, K. (2014). Heterogeneous catalysis for sustainable biodiesel production via esterification and transesterification. **Chemical Society Reviews**. 43(22): 7887–7916.

Liu, N., Wu, Z., Li, M., Li, S., Li, Y., Yu, R., Pan L. and Liu, Y. (2017b). A novel strategy for constructing mesoporous solid superbase catalysts: Bimetallic Al-La oxides supported on SBA-15 modified with KF. **Catalysis Science and Technology**. 7(3): 725–733.

Liu, N., Wu, Z., Li, M., Li, S., Luo, Z., Li, Y., Pan, L. and Liu, Y. (2017a). Low-Temperature Preparation of a Mesoporous Silica Superbase by Employing the Multifunctionality of a La_2O_3 Interlayer. **ChemCatChem**. 9(9): 1641–1647.

Liu, X.-Y., Sun, L. B., Lu, F., Li, T. T. and Liu, X. Q. (2013). Constructing mesoporous solid superbases by a dualcoating strategy. **Journal of Materials Chemistry A**. 1(5): 1623–1631.

Mack, P. (2019). **Spectroscopic analysis of solid oxide fuel cell material with XPS (Thermo Fisher Scientific Application Note: 52110)** [On-line]. Available: http://tools.thermofisher.com/content/sfs/brochures/AN52110-E-SolidOxid eFuelCell0511MH.pdf

Mahmudul, H. M., Hagos, F. Y., Mamat, R., Adam, A. A., Ishak, W. F. W. and Alenezi, R. (2017). Production, characterization and performance of biodiesel as an alternative fuel in diesel engines – A review. **Renewable and Sustainable Energy Reviews**. 72: 497–509.

Manadee, S., Sophiphun, O., Osakoo, N., Supamathanon, N., Kidkhunthod, P., Chanlek, N., Wittayakun, J. and Prayoonpokarach, S. (2017). Identification of potassium phase in catalysts supported on zeolite NaX and performance in transesterification of Jatropha seed oil. **Fuel Processing Technology**. 156: 62–67.

Mansir, N., Taufiq-Yap, Y. H., Rashid, U. and Lokman, I. M. (2017). Investigation of heterogeneous solid acid catalyst performance on low grade feedstocks for biodiesel production: A review. **Energy Conversion and Management**. 141: 171–182. **Mesoporous Materials**. 230: 66–75.

Neimark, A. V., Thommes, M., Sing, K. S. W., Rodriguez-Reinoso, F., Olivier, J. P., Kaneko, K. and Rouquerol, J. (2015). Physisorption of gases, with special reference to the evaluation of surface area and pore size distribution (IUPAC Technical Report). **Pure and Applied Chemistry**. 87: 1051–1069.

Rakmae, S., Keawkumay, C., Osakoo, N., Montalbo, K. D., de Leon, R. L., Kidkhunthod, P., Chanlek, N., Roessner, F., Prayoonpokarach, S. and Wittayakun, J. (2016). Realization of active species in potassium catalysts on zeolite NaY prepared by ultrasound-assisted impregnation with acetate buffer and improved performance in transesterification of palm oil. **Fuel**. 184: 512–517.

Roschat, W., Siritanon, T., Yoosuk, B., Sudyoadsuk, T. and Promarak, V. (2017). Rubber seed oil as potential non-edible feedstock for biodiesel production using heterogeneous catalyst in Thailand. **Renewable Energy**. 101: 937–944.

Saad, A., Snoussi, Y., Abderrabba, M. and Chehimi, M. M. (2016). Ligand-modified mesoporous silica SBA-15/silver hybrids for the catalyzed reduction of methylene blue. **RSC Advances**. 6(62): 57672–57682.

Sharma, Y. C., Singh, B. and Korstad, J. (2011). Latest developments on application of heterogenous basic catalysts for an efficient and eco friendly synthesis of biodiesel: A review. **Fuel**. 90(4): 1309–1324.

Soltani, S., Rashid, U., Al-Resayes, S. I. and Nehdi, I. A. (2017). Recent progress in synthesis and surface functionalization of mesoporous acidic heterogeneous catalysts for esterification of free fatty acid feedstocks: A review. **Energy Conversion and Management**. 141: 183–205.

Sun, L. B., Kou, J. H., Chun, Y., Yang, J., Gu, F. N., Wang, Y., Zhu, J. H. and Zou, Z. G. (2008). New attempt at directly generating superbasicity on mesoporous silica SBA-15. **Inorganic Chemistry**. 47(10): 4199–4208.

Sun, L. B., Liu, X. Q. and Zhou, H. C. (2015). Design and fabrication of mesoporous heterogeneous basic catalysts. **Chemical Society Reviews**. 44(15): 5092–5147.

Sun, Y. H., Sun, L. B., Li, T. T. and Liu, X. Q. (2010). Modulating the host nature by coating alumina: A strategy to promote potassium nitrate decomposition and superbasicity generation on mesoporous silica SBA-15. **Journal of Physical Chemistry C**. 114(44): 18988–18995.

Supamathanon, N., Wittayakun, J. and Prayoonpokarach, S. (2011). Properties of Jatropha seed oil from Northeastern Thailand and its transesterification catalyzed by potassium supported on NaY zeolite. **Journal of Industrial and Engineering Chemistry**. 17(2): 182–185.

Supamathanon, N., Wittayakun, J., Prayoonpokarach, S., Roessner, F. and Supronowicz, W. (2012). Basic properties of potassium oxide supported on zeolite y studied by pyrrole-tpd and catalytic conversion of methylbutynol. **Química Nova**. 35(9): 1719–1723.

Wang, F., Ta, N., Li, Y. and Shen, W. (2014). La(OH)$_3$ and La$_2$O$_2$CO$_3$ nanorod catalysts for Claisen-Schmidt condensation. **Chinese Journal of Catalysis**. 35(3): 437–443.

Wang, X., Sun, T., Yang, J., Zhao, L. and Jia, J. (2008). Low-temperature H$_2$S removal from gas streams with SBA-15 supported ZnO nanoparticles. **Chemical Engineering Journal**. 142(1): 48–55.

Wang, X., Wang, M., Song, H. and Ding, B. (2006). A simple sol–gel technique for preparing lanthanum oxide nanopowders. **Materials Letters**. 60: 2261–2265.

Wu, H., Zhang, J., Liu, Y., Zheng, J. and Wei, Q. (2014). Biodiesel production from Jatropha oil using mesoporous molecular sieves supporting K$_2$SiO$_3$ as catalysts for transesterification. **Fuel Processing Technology**. 119: 114–120.

Wu, Z. Y., Jiang, Q., Wang, Y. M., Wang, H. J., Sun, L. B., Shi, L. Y., Xu, J. H., Wang Y., Chun Y. and Zhu, J. H. (2006). Generating superbasic sites on mesoporous silica SBA-15. **Chemistry of Materials**. 18(19): 4600–4608.

Xie, W. and Li, H. (2006). Alumina-supported potassium iodide as a heterogeneous catalyst for biodiesel production from soybean oil. **Journal of Molecular Catalysis A: Chemical**. 255(1–2): 1–9.

Zhao, D., Feng, J., Huo, Q., Melosh, N., Fredrickson, G. H., Chmelka, B. F. and Stucky, G.D. (1998). Triblock copolymer syntheses of mesoporous silica with periodic 50 to 300 angstrom pores. **Science**. 279(5350): 548–552.

APPENDIX
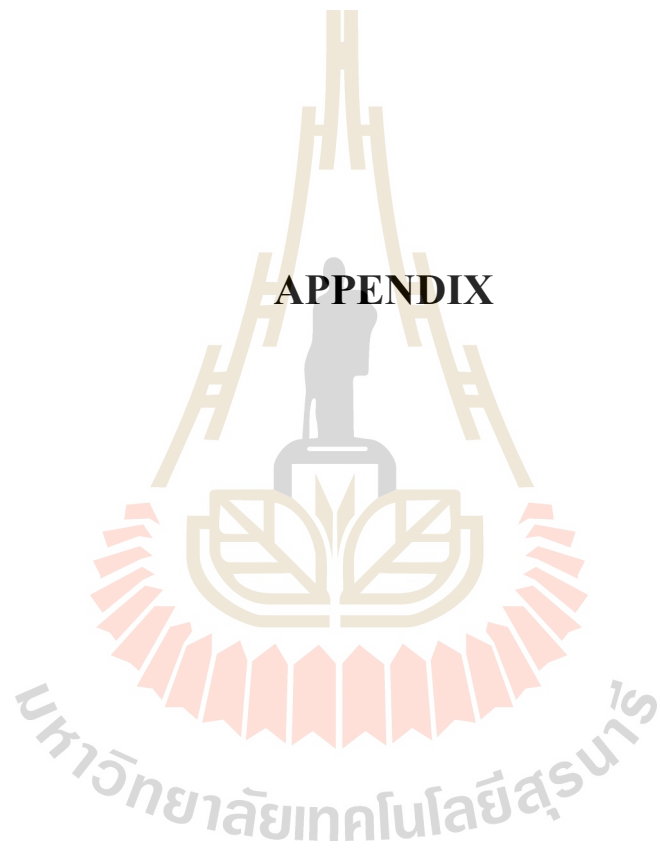
APPENDIX

PREPARATION OF POTASSIUM SUPPORTED ON

Al-SBA-15 FOR TRANSESTERIFICATION

OF PALM OIL

Introduction

Zeolite Y (NaY) was impregnated with 12wt.% K by using potassium acetate buffer as potassium precursor to identify active species (Rakmae et al., 2016). They found that potassium active phase prepared form potassium acetate buffer was potassium carbonate (K_2CO_3). The catalyst was tested in transesterification of refined palm oil to produce biodiesel with the yield of 72% at 60°C within 2 h. However, NaY sorption dimensionality, 0.34 nm (Baerlocher and McCusker, 2007), is smaller than the estimated three-dimension of triglyceride, 2.4 nm (Harrison, 2007). Thus, the diffusion of triglyceride to active site in the pore of NaY is limited. To improve the diffusion, mesoporous material with a larger pore size than zeolite is employed as a support in this work.

There are some reports about potassium on mesoporous material such as MCM-41. MCM-41 is mesoporous material composed of silica. Loading potassium on MCM-41 by using potassium acetate as precursor (Artkla et al., 2008) and potassium acetate buffer (Supamathanon, 2011) resulted in the collapse of MCM-41 structure. The collapsed catalysts were tested on transesterification. The results indicate that the

collapsed catalyst could produce FAME although the reaction was not complete (Artkla et al., 2008; Supamathanon, 2011). Due to the collapse of MCM-41 after loading potassium, the other mesoporous material should be employed.

SBA-15 is silica with hexagonal array of mesopore containing size between 2-10 nm (Alothman, 2012). With a large pore size, SBA-15 is selected as a support to reduce mass transfer limitation and improve the catalytic activity of transesterification. However, SBA-15 acts as only a support and does not involve in catalysis. The incorporation of Al into SBA-15 framework generated Brønsted and Lewis acid site confirmed by FTIR spectroscopy of pyridine adsorption (Li et al., 2004). Compared the transesterification activity, the FAME yield of canola oil produced from Al-SBA-15 was four times higher than SBA-15 (Liang et al., 2013). From the good catalytic performance, Al-SBA-15 is employed as the support in this work.

To study the effect of pore size of support on the catalytic performance in transesterification, Al-SBA-15 is prepared by incorporating Al into the SBA-15 structure to generate Brønsted and Lewis acid site. 12wt.% K supported on Al-SBA-15 is prepared via incipient wetness impregnation by using potassium acetate buffer as potassium precursor to acquire K_2CO_3 as active species according to Rakmae et al. (2016). 12wt.% K on Al-SBA-15 is tested in transesterification of palm oil to determine its catalytic performance in biodiesel production. The performance of K on Al-SBA-15 is compared with 12wt.% K on NaY reported from Rakmae et al. (2016) to decide the effect of support pore size.

Materials and methods

The chemicals used for Al-SBA-15 synthesis included poly (ethylene glycol)-block-poly(proplylene glycol)-block-poly(ethylene glycol) (P123, $M_n \sim 5800$, Sigma-Aldrich), tetraethyl orthosilicate (TEOS, 98%, Sigma-Aldrich), aluminium isopropoxide ($Al(OCH(CH_3)_2)_3$, >98%, Acros Organics) and hydrochloric acid (HCl, AR grade, Sigma-Aldrich). The chemicals for preparation of potassium acetate buffer were potassium acetate (CH_3COOK, ACS grade, Carlo Erba) and acetic acid (CH_3COOH, 99.7%, RCI Labscan). The chemicals for transesterification palm oil were refined palm oil (palm olein type) and methanol (CH_3OH, HPLC grade, Honeywell Riedel-de Haën). The chemicals for thin layer chromatography (TLC) testing were TLC plate (Silica Gel 60 F_{254}, Merck), petroleum ether (Panreac), diethyl ether (($C_2H_5)_2O$, 99.7%, Panreac) and acetic acid (CH_3COOH, 99.7%, RCI Labscan).

Synthesis of Al-SBA-15 and preparation of K/Al-SBA-15

Al-SBA-15 was synthesized via hydrothermal method by the procedure and condition from literature (Kocík et al., 2017) with half scale of the original synthesis. P123 (5 g) was dissolved in deionized water (75 cm^3) and protonated with 2 M HCl (75 cm^3) under stirring at 40°C for 3 h. The solution of aluminum isopropoxide (0.417 g) in 2 M HCl (12.5 cm^3) and tetraethyl orthosilicate (10 g) were added dropwise to the P123 solution to obtain the gel with molar ratio of Si/Al = 25. The solution was stirred continuously at 40°C for 24 h. Then, the solution was transferred to a Teflon-lined stainless steel autoclave, heated to 95°C and held for 48 h. The obtained solid was separated by centrifugation washed by deionized water until the pH of the washed solution equaled to the pH of deionized water (pH 5.5), dried overnight at 90°C and

calcined at 550°C for 6 h to remove the template. The sample was named as Al-SBA-15.

12 wt.% K supported on Al-SBA-15 was prepared by the procedure modified from Rakmae et al. (2016) by using potassium acetate buffer as potassium precursor. The buffer solution was prepared with these following steps. CH_3COOK (1.4230 g) was dissolved in deionized water (5 cm^3). Then, 1 M CH_3COOH (17.5 cm^3) was added and the volume was adjusted to 25 cm^3 by deionized water. The buffer solution (6 cm^3) was dropped to 1 g of Al-SBA-15 to obtain 12wt.% of potassium. The mixture was dried at 80°C overnight, then calcined at 550°C for 6 h. The resulting materials was named as K/Al-SBA-15.

Characterization of Al-SBA-15 and K/Al-SBA-15

The synthesized Al-SBA-15 and K/Al-SBA-15 were analyzed by X-ray diffraction on a Bruker D8 Advance with monochromatic light source Cu Kα (wavelength 1.5418 Å). The sample was analyzed at 2θ = 0.5-10 degree by using scan speed 1.0 s/step and increment 1.0 s/step and scan speed 0.5 s/step.

Morphology of Al-SBA-15 and K/Al-SBA-15 were studied by transmission electron microscopy (FEI Tecnai G^2) at electron acceleration voltage 200 kV. The samples were dispersed in ethanol and then sonicated for 5 min. The mixture was dropped on the carbon-coated copper grid for the measurement.

Catalytic testing on transesterification of palm oil

12wt.% K on Al-SBA-15 was tested for transesterification of palm oil with procedure from Rakmae et al. (2016) in a round bottom flask equipped with water

cooled condenser. The refined palm oil (5 g) was stirred at 250 rpm and heated to 60°C. Then, methanol (2.9 g) and catalyst (0.2 g) was added in the oil. The mixture was continuously stirred at 60°C for 3 h. The mixture was hot filtered (Whatman No.5) to separate catalyst from solution. The filtered solution was evaporated to remove methanol by rotary evaporator at 50°C. Then, the solution was transferred into a separatory funnel and left to separate into two layers: palm oil and fatty acid methyl ester in the upper layer and glycerol in the bottom layer. The upper layer solution was spotted on TLC plate for preliminary result of catalytic activity by using solution of petroleum ether/diethyl ether/glacial acetic acid (volume ratio of 85:15:1) as a mobile phase (Supamathanon et al., 2011).

Results and Discussion

Preparation of K/Al-SBA-15

Figure 1 shows XRD patterns of Al-SBA-15 and K/Al-SBA-15. The pattern of Al-SBA-15 consists of peaks at 0.9°, 1.5°, 1.7°, 2.3° and 2.6 °attributing to (100), (110), (200) (210) and (300) planes, respectively. The peaks correspond to P6mm hexagonal symmetry (Zhao et al., 1998) similar to that of siliceous SBA-15. The results also agree well with the reference synthesis of SBA-15 (Kocík et al., 2017) confirming that the synthesis of Al-SBA-15 with half-scale was successful.

In contrast, the XRD pattern of K/Al-SBA-15 does not show the characteristic peaks of SBA-15 indicating that the structure collapses after loading potassium. There are reports about the collapse of potassium of potassium-loaded mesoporous silica after calcination. Potassium was loaded into MCM-41 by using potassium acetate (Artkla et al., 2008) and potassium acetate buffer (Supamathanon, 2011) as potassium precursor.

The results of both works indicate that the structure of MCM-41 collapsed after calcination. It suggests that the mesoporous silica with Al (Al-SBA-15) and without Al (MCM-41) collapses when loading with potassium.
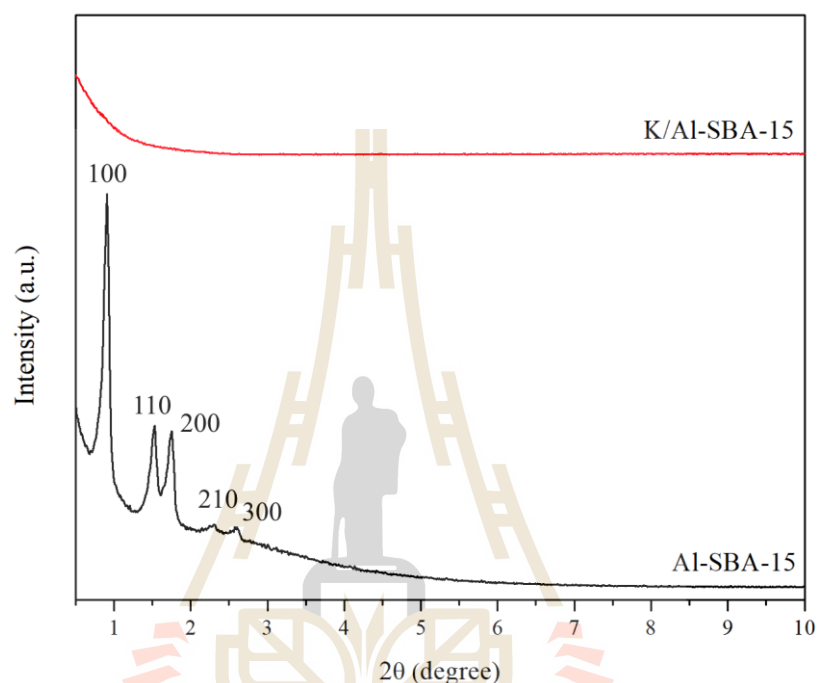
Figure 1 XRD patterns of Al-SBA-15 and K/Al-SBA-15 prepared with potassium acetate buffer.

Figure 2(a) and (b) shows TEM of Al-SBA-15 exhibiting the array of long rods with the width about 1.7 nm. Figure 2(c) shows the hexagonal arrangement of pore with pore diameter about 10 nm and wall thickness 4 nm. The wall thickness of synthesized Al-SBA-15 is close to SBA-15 which around 3-5 nm (Zhao et al., 1998) and is also the same thickness as Al-SBA-15 reported form Li et al. (2004) and Li et al. (2010).

Figure 3(a)-(c) shows TEM images of K/Al-SBA-15 indicating that Al-SBA-15 rods (a)-(b) and pores (c) are destroyed and become the particles with irregular shape

of space inside. The TEM images of K/Al-SBA-15 are consistent with the XRD result. The loaded SBA-15 with ZrO_2 were impregnated with potassium nitrate (Liu et al. 2013). The results indicate that the structure of SBA-15 collapsed after calcination confirmed by XRD result and TEM images. The TEM image of K/ZrO_2-SBA-15 is similar to Figure 3(a) K/Al-SBA-15. This suggests that the destruction of siliceous framework has the same morphology.

Sun and co-workers (2008) prepared various catalysts by impregnation of nitrate salts of alkali metal including $NaNO_3$, KNO_3 and $CsNO_3$ into SBA-15, and then calcination at 550°C to convert the nitrate salt to metal oxide. As a result, the structure of SBA-15 impregnated with alkali precursors collapsed after calcination. They suggested that the mobility in term of the diffusion of metal oxide into the pore of silica, occurs at high temperature, causes acceleration of the reaction between basic oxide and silica support which leads to the destruction of support. The mobility of metal oxide raises rapidly at its Tammann temperature, defined as a half of melting point. The alkali metal oxides have the Tammann temperature <430°C which lower the calcined temperature, so they are active or great diffusion into the pore of silica. Potassium carbonate, the active species for this work, has melting point at 899°C (Haynes et al., 2015) so that its Tammann temperature is 444.5°C which lower than the calcined temperature. Thus, potassium carbonate may also great diffuse into the pore of Al-SBA-15 resulting in the destruction of Al-SBA-15.
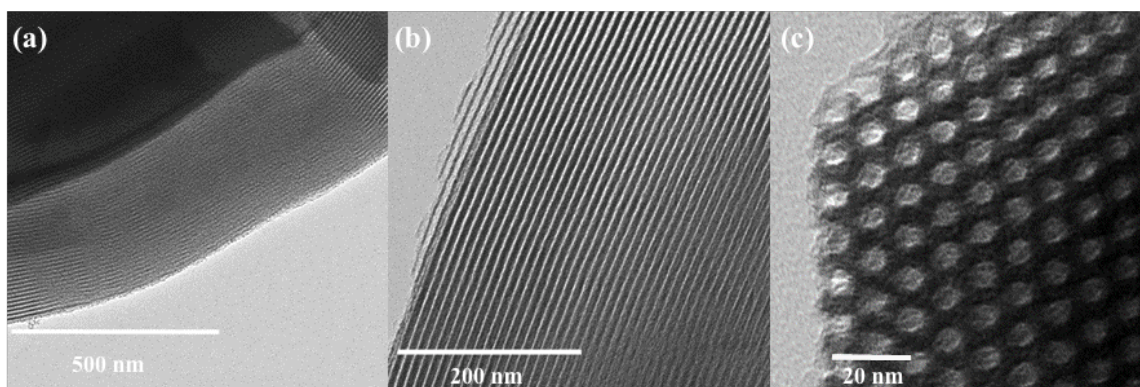
Figure 2 TEM image of (a) and (b) Al-SBA-15 rods and (c) Al-SBA-15 pores.
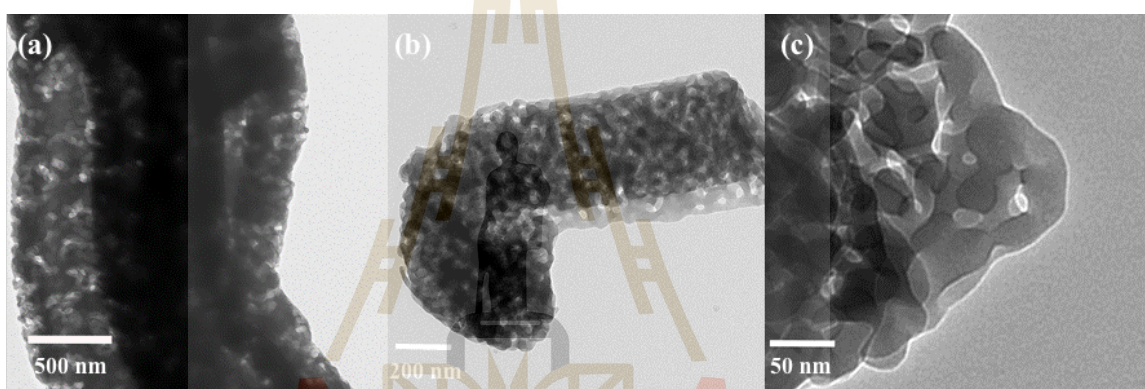
Figure 3 TEM image of K/Al-SBA-15 prepared with potassium acetate buffer.

Catalytic testing: transesterification for biodiesel production

12wt.% K/Al-SBA-15 with potassium acetate buffer as K precursor were tested their catalytic performance in transesterification of palm oil. The palm oil used as reactant and the upper layer product were spotted on TLC plate shown in Figure 4 to determine conversion of palm oil. Palm oil converted to fatty acid methyl ester around 40% estimated from the spots. K/Al-SBA-15 can catalyze the reaction and produce methyl ester even its structure destroyed. Compared with transesterification of palm oil over 12wt.% K supported on NaY, the biodiesel yield was 72.4% reported by Rakmae

et al. (2016). The catalytic performance of K supported on Al-SBA-15 is lower. It may result from the collapse of support structure.

Supamethanon (2011) prepared 8wt.% K on MCM-41 by using potassium acetate buffer as potassium precursor and tested on transesterification of extracted Jatropha seed oil. The catalyst could produce FAME about 70% estimated form TLC plate. The performance of K on MCM-41 is higher than K on Al-SBA-15 in this work. However, both Al-SBA-15 and MCM-41 structure collapse after loading potassium.

Artkla et al. (2008) has studied catalytic activity of potassium acetate on MCM-41 and rice husk silica calcined at 500°C on transesterification of palm oil. The catalytic performance of K on MCM-41 with partial collapse structure gave remarkably higher conversion than K on silica due to the remained mesoporous structure and the higher surface area. It suggests that the mesoporous structure and surface area are importance for the catalytic performance.

The proposed catalyst to improve the diffusion of triglyceride by using mesoporous material as support cannot be concluded because collapse of the structure of Al-SBA-15. To confirm the role of mesopore on the catalytic performance, the catalyst without collapse of the support should be prepared.
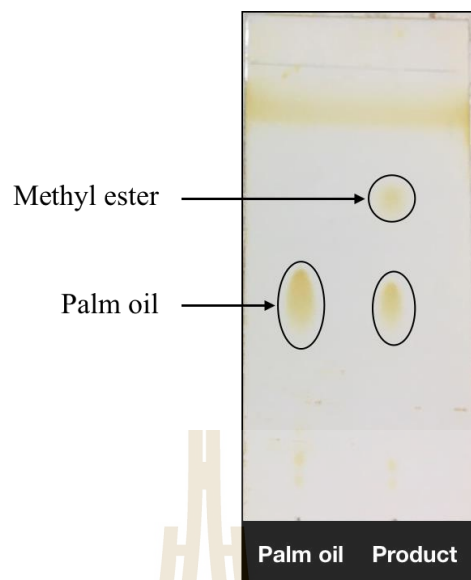
Figure 4 TLC results of upper layer biodiesel produced over 12wt.% K/Al-SBA-15 with potassium acetate buffer as K precursor.

Conclusions

Al-SBA-15 with Si/Al ratio 25 was successfully synthesized. However, the structure collapses after loading potassium. The collapse of structure cannot be avoided if K is directly loaded on Al-SBA-15. 12wt.% K/Al-SBA-15 with collapse structure is tested in transesterification to produce biodiesel. The catalyst can catalyze palm oil and methanol to fatty acid methyl ester through transesterification although the reaction is not complete. The procedure to prepare K supported on Al-SBA-15 without structure collapse should be carried out to improve the performance of the catalyst.

References

Alothman, Z. A. (2012). A review: Fundamental aspects of silicate mesoporous materials. **Materials**. 5(12): 2874–2902.

Artkla, S., Grisdanurak, N., Neramittagapong, S. and Wittayakun, J. (2008). Characterization and catalytic performance on transesterification of palm olein of potassium oxide supported on RH-MCM-41 from rice husk silica. **Suranaree Journal of Science and Technology**. 15(2): 133–138.

Baerlocher, Ch. and McCusker L. B. (2007). **Framework type FAU** [On-line]. Available: https://asia.iza-structure.org/IZA-SC/framework.php?STC=FAU

Harrison, K. (2007). **Triglyceride (Molecule of the Month for March 2007)** [On-line]. Available: http://www.3dchem.com/Triglyceride.asp

Haynes, W.M., Lide, R. D. and Bruno, J. T. (Ed.). (2015). **CRC Handbook of Chemistry and Physics: A Ready Reference Book of Chemical and Physics Data, 96th Edition**. Boca Raton, Florida: CRC Press.

Kocík, J., Samikannu, A., Bourajoini, H., Pham, T. N., Mikkola, J.-P., Hájek, M. and Čapek, L. (2017). Screening of active solid catalysts for esterification of tall oil fatty acids with methanol. **Journal of Cleaner Production**. 155: 34–38.

Li, Q., Wu, Z., Tu, B., Park, S. S., Ha, C. S. and Zhao, D. (2010). Highly hydrothermal stability of ordered mesoporous aluminosilicates Al-SBA-15 with high Si/Al ratio. **Microporous and Mesoporous Materials**. 135: 95–104.

Li, Y., Zhang, W., Zhang, L., Yang, Q., Wei Z., Feng, Z. and Li, C. (2004). Direct synthesis of Al-SBA-15 mesoporous materials via hydrolysis-controlled approach. **Journal of Physical Chemistry B**. 108(28): 9739–9744.

Liang, C., Wei, M. C., Tseng, H. H. and Shu, E. C. (2013). Synthesis and characterization of the acidic properties and pore texture of Al-SBA-15 supports for the canola oil transesterification. **Chemical Engineering Journal**. 223: 785–794.

Liu, X.-Y., Sun, L. B., Lu, F., Li, T. T. and Liu, X. Q. (2013). Constructing mesoporous solid superbases by a dualcoating strategy. **Journal of Materials Chemistry A**. 1(5): 1623–1631.

Rakmae, S., Keawkumay, C., Osakoo, N., Montalbo, K. D., de Leon, R. L., Kidkhunthod, P., Chanlek, N., Roessner, F., Prayoonpokarach, S. and Wittayakun, J. (2016). Realization of active species in potassium catalysts on zeolite NaY prepared by ultrasound-assisted impregnation with acetate buffer and improved performance in transesterification of palm oil. **Fuel**. 184: 512–517.

Sun, L. B., Kou, J. H., Chun, Y., Yang, J., Gu, F. N., Wang, Y., Zhu, J. H. and Zou, Z. G. (2008). New attempt at directly generating superbasicity on mesoporous silica SBA-15. **Inorganic Chemistry**. 47(10): 4199–4208.

Supamathanon, N. (2011**). Biodiesel production via transesterification of Jatropha seed oil using potassium supported on NaY zeolite and MCM-41 as catalysts**. Ph.D. Dissertation, Suranaree University of Technology, Nakhon Ratchasima, Thailand.

Supamathanon, N., Wittayakun, J. and Prayoonpokarach, S. (2011). Properties of Jatropha seed oil from Northeastern Thailand and its transesterification catalyzed by potassium supported on NaY zeolite. **Journal of Industrial and Engineering Chemistry**. 17(2): 182–185.

Zhao, D., Feng, J., Huo, Q., Melosh, N., Fredrickson, G. H., Chmelka, B. F. and Stucky, G.D. (1998). Triblock copolymer syntheses of mesoporous silica with periodic 50 to 300 angstrom pores. **Science**. 279(5350): 548–552.

CURRICULUM VITAE

Name Miss Nopphawan Bunthiam

Education

2016-present   M.Sc. student (Chemistry) Suranaree University of

Technology, Thailand

2015   B.Sc. (Chemistry, First class honours), Khon Kaen

University, Thailand

Research exchange experience

April 2018-June 2018   Research about MBOH catalytic conversion at Carl von

Ossietzky Universität Oldenburg, Germany

Scholarship

2009-present   Development and Promotion of Science and

Technology Talents Project (DPST)